Pointwise numerical simulation of one-dimensional fractional sine-Gordon model in time-dependent variable using reproducing kernel Hilbert algorithm

Omar Abu Arqub [1,2,*], Jagdev Singh [2,3], Mohammed Alhodaly [2], Tasawar Hayat [2,4]

[1] Department of Mathematics, Faculty of Science, Al-Balqa Applied University, Salt 19117, Jordan
[2] Nonlinear Analysis and Applied Mathematics (NAAM) Research Group, Department of Mathematics, Faculty of Science, King Abdulaziz University, Jeddah 21589, Saudi Arabia
[3] Department of Mathematics, JECRC University, Jaipur-303905, Rajasthan, India
[4] Department of Mathematics, Faculty of Science, Quaid-I-Azam University, Islamabad 45320, Pakistan

[*] Corresponding author: Omar Abu Arqub, e-mail: o.abuarqub@bau.edu.jo

Abstract. In this study, the fractional sine-Gordon model in the time-dependent variable domain using Caputo non-integer order basis derivative is presented. The main purpose is to utilize the adaptation of reproducing kernel Hilbert algorithm to construct pointwise numerical solution to variant forms of fractional sine-Gordon model in fullness of overdetermination Dirichlet boundary condition. Allocates theoretical requirements are employed to interpret pointwise numerical solutions to such fractional models on the space of Sobolev. In addendum, the convergence of the pointwise numerical algorithm and error estimates are promoted by global convergence treatises. This handling pointwise numerical solution depending on the orthogonalization Schmidt process that can be straightway carried out to generate Fourier expansion within a fast convergence rate. The soundness and powerfulness of the discussed algorithm are expounded by testing the solvability of a couple of time-fractional sine-Gordon models. Some schematic plots and tabulated results outcomes signalize that the algorithm procedure is accurate and convenient in the field of fractional sense. Ultimately, future remarks and concluding are acted with the most focused used references.

Keywords: Time-fractional sine-Gordon model; Dirichlet boundary condition; Reproducing kernel Hilbert algorithm; Caputo time-fractional partial derivative; Pointwise numerical solution

Abbreviations: TFSGM: Time-fractional sine-Gordon model; DBC: Dirichlet boundary condition; RKHA: reproducing kernel Hilbert algorithm; CTFPD: Caputo time-fractional partial derivative; HS: Hilbert space; RK: Reproducing kernel

1 Utilization

The physical constructions of TFSGM concern an interdisciplinary field connecting mathematical analysis, numerical mathematics, semiclassical physics, and quantum physics, which are designed and analyzed to simulate physical behaviors in modern wave theory, models of particle physics, stability of fluid motions, nonlinear optics, differential geometry, and propagation of fluxon [1-9]. But in return, the sources why we examine the fractional kind of SGM are that: in the real phenomena, the following state of a physical mode relies on not exclusive its existing state but also at its historical states. To paradigm such characteristics and merits, a robust and adequate tool is the fractional descriptive approach. This signalizes that, TFSGM can supply a lot more precise and appropriate depiction of the physical modes including hereditary and memory characteristics. Generally, the fractional descriptive approach lids many scopes of engineering and science such as anomalous diffusion, biological models, quantum mechanics, Pipkin's viscoelasticity, etc. [10-14].

So that more and more fractional systems have been utilized lately, a way to assemble the solutions of fractional integral/differential models becomes a crucial and warm subject. But in return, for widely of such fractional integral/differential models, we cannot reap their analytic solutions in terms of well-known basic functions. Thereafter, a huge quantity of researchers has attempted to broaden numerical schemes, approximation methods, or numerical algorithms to manage answers which might be lacking or tough to find. Focusing on these findings, we can see it's far an exciting and difficult challenge to broaden numerical methods for such fractional

integral/differential models. In this analysis, we utilize and design an efficient and fast numerical algorithm in the space of Sobolev relying on RK Hilbert functions, so-called, the RKHA to solve the TFSGM regarding the DBC in form of schematic plot and tabulated results. Anyhow, we consider the subsequent fractional model that obey the following formalism:

$$\partial_{\tau}^{\omega}\phi(\kappa,\tau)+\mathcal{A}\,\partial_{\tau}\phi(\kappa,\tau)-\mathcal{B}\,\partial_{\kappa}^{2}\phi(\kappa,\tau)+\upsilon(\kappa,\tau)\sin\big(\phi(\kappa,\tau)\big)=\psi(\kappa,\tau), \tag{1}$$

regarding the DBC

$$\begin{cases}\phi(\kappa,0)=\varphi_1(\kappa),\\ \partial_{\tau}\phi(\kappa,0)=\varphi_2(\kappa),\\ \phi(0,\tau)=\chi_1(\tau),\\ \phi(1,\tau)=\chi_2(\tau),\end{cases} \tag{2}$$

and regarding the CTFPD

$$\partial_{\tau}^{\omega}\phi(\kappa,\tau)=\begin{cases}\Gamma^{-1}(2-\omega)\int_0^{\tau}(t-\omega)^{1-\alpha}\,\partial_t^2\phi(\kappa,t)dt, & 1<\omega<2,\\ \partial_{\tau}^{2}\phi(\kappa,\tau), & \omega=2.\end{cases} \tag{3}$$

Herein, $(\kappa,\tau)\in\Omega:=[0,1]\times[0,1]$, $\upsilon(\kappa,\tau)$ and $\psi(\kappa,\tau)$ are smooth enough functions defined on Ω, and $\partial_{\tau}^{\omega}\phi(\kappa,\tau)$ with $1<\omega<2$ represent the CTFPD of $\phi(\kappa,\tau)$ over the measurement interval $0\le t<\tau\le 1$. The term parameters $\mathcal{A}$ and $\mathcal{B}$ are known as the dissipative with $\mathcal{A}\ge 0$ and $\mathcal{B}>0$. Specifically, TFSGM (1-3) reduces to undamped TFSGM for $\mathcal{A}=0$ and a damped one for $\mathcal{A}>0$. The term function $\upsilon(\kappa,\tau)$ represents Josephson current density, whilst, $\varphi_1(\kappa)$ and $\varphi_2(\kappa)$ characterize wave models and velocity, simultaneously. In addendum to the previous, $\psi(\kappa,\tau)$ is known as the forcing non-homogenized function, whilst $\chi_1(\tau)$ and $\chi_2(\tau)$ are boundary forcing functions. Hither, by $\partial_{\tau}\phi(\kappa,\tau)$ we mean $\phi_{\tau}(\kappa,\tau)$ and by $\partial_{\kappa}^{2}\phi(\kappa,\tau)$ we mean $=\phi_{\kappa\kappa}(\kappa,\tau)$, and so on.

Mathematically, the DBC is a type of constraint solution that commonly appears when imposed on the differential/integral models, it is an apportionment of a linear interpolation of the values of a suggested solution on Ω. As a rule, DBC is a weighted interpolation of Robin-Neumann BCs. This constraint is rendered as impedance conditions, from their fulfillment in electrostatics, thermodynamics, fluid dynamics, and beam theory [15-29]. Anyhow, an interesting type of TFSGM is finding an unknown source term function $\phi(\kappa,\tau)$ behind conformable DBC of its component as utilized in (1-3). In this permission, we are interested in finding a pointwise numerical solution $\phi_n(\kappa_l,\tau_m)$ whose seek behind unique exact one and its DBC.

On the numerical level, the RKHA was used in its discretion horizon to pointwise numerically solving and studying bifurcations behavior of a variety of integral/differential operator models of different species of derivatives [30-52]. More specifically, the implementation of the RKHA for pointwise numerical solvability of TFSGM depends on four phases as [53-55]:

- Firstly, we neatly identify solution domain-range spaces whereas an unsuitable choice is an obstacle to achieve the coveted solutions.
- Secondly, we erect the RK functions whereas the focusing is on the Green function positionality.
- Thirdly, we generate a group of orthonormal basis functions for space solutions by couple RK functions, Gram-Schmidt orthogonalization process, a boundary operator, and a dense sequence of points in the domain of space solution.
- Fourthly, we symbolize the exact continued answer of TFSGM by a sum of an infinite orthonormal basis functions accomplished from the mentioned last stages.
- Finally, we truncate series of exact solution representation by n-terms as a numerical pointwise solution.

In contract of the utilization, the enduring sections are synopsized sequentially as next: Section 2 utilized fundamentals RK spaces and RK functions. Section 3 utilized the preparation and processing of TFSGM in RKHA. Section 4 utilized convergence of solutions in RKHA and some addendum results. Section 5 utilized RKHA junctures and mathematical debates with some tabulation and plot results. Ultimately, Section 7 utilized highlight, concluding, and future.

2 Fundamentals RK spaces and RK functions

If H is an HS of mappings defined on a set Δ, then $T:\Delta\times\Delta\to\mathbb{R}$ is an RK of H when the next are completely fulfilled:

Firstly, for each $\tau \in \Delta, \mathrm{T}(\cdot,\tau) \in \mathrm{H}$. Secondly, for each $\mathrm{T} \in \mathrm{H}$ and each $t \in \Delta, \langle \mathrm{T}(\cdot), \mathrm{T}(\cdot,\tau)\rangle_{\mathrm{H}} = \mathrm{T}(\tau)$. Hither, we will write $\|\omega\|_{\zeta}^2 = \langle \omega(\xi), \omega(\xi)\rangle_{\zeta}$ with $\omega \in \zeta$, $\xi \in [0,1]$ and $\zeta \in \{\Sigma_{(1,2)}, \hat{\Sigma}_{(1,2)}, \Sigma_{(3,2)}, \hat{\Sigma}_{(3,2)}\}$. In addendum, we will assume that $\omega, \omega', \omega'' \in L^2[0,1]$, whilst, $AC[0,1]$ denotes the set of absolutely continuous functions on $[0,1]$.

The elements in $\Sigma_{(1,2)}$ are explored as $\Sigma_{(1,2)}[0,1] = \{\chi: \chi \in AC[0,1]\}$ and equipped with the inner representation product

$$\langle \chi_1(\tau), \chi_2(\tau)\rangle_{\Sigma_{(1,2)}} = \chi_1(0)\chi_2(0) + \int_0^1 \chi_1'(\tau)\chi_2'(\tau)d\tau. \tag{4}$$

But in return, the RK function of $\Sigma_{(1,2)}[0,1]$ can performs as

$$\Pi_{\varsigma}^{\{1\}}(\tau) = 1 + \min(\varsigma, \tau). \tag{5}$$

In the identical modality, if $[0,1]$ is the domain-space, then the inner representation product of $\hat{\Sigma}_{(1,2)}[0,1]$ has the form $\langle \varphi_1(\kappa), \varphi_2(\kappa)\rangle_{\hat{\Sigma}_{(1,2)}} = \varphi_1(0)\varphi_2(0) + \int_0^1 \varphi_1'(\kappa)\varphi_2'(\kappa)d\kappa$ with RK function $\hat{\Pi}_{\lambda}^{\{1\}}(\kappa) = 1 + \min(\kappa, \lambda)$.

The elements in $\Sigma_{(3,2)}$ are explored as $\Sigma_{(3,2)}[0,1] = \{\chi: \chi, \chi' \in AC[0,1] \wedge \chi(0) = \chi'(0) = 0\}$ and equipped with the inner representation product

$$\langle \chi_1(\kappa), \chi_2(\kappa)\rangle_{\Sigma_{(3,2)}} = \sum_{i=0}^{2} \chi_1^{(i)}(0)\chi_2^{(i)}(0) + \int_0^1 \chi_1''(\tau)\chi_2''(\tau)d\tau. \tag{6}$$

But in return, the RK function of $\Sigma_{(3,2)}[0,1]$ can performs as

$$\Pi_{\varsigma}^{\{3\}}(\tau) = \frac{1}{120}\begin{cases} \tau^2\big(\tau^3 - 5\tau^2\varsigma + 10\varsigma^2(\tau+3)\big), & \tau \le \varsigma, \\ \varsigma^2\big(\varsigma^3 - 5\varsigma^2\tau + 10\tau^2(\varsigma+3)\big), & \tau > \varsigma. \end{cases} \tag{7}$$

The elements in $\hat{\Sigma}_{(3,2)}$ are explored as $\hat{\Sigma}_{(3,2)}[0,1] = \{\varphi: \varphi, \varphi', \varphi'' \in AC[0,1] \wedge \varphi(0) = \varphi(1) = 0\}$ and equipped with the inner representation product

$$\langle \varphi_1(\kappa), \varphi_2(\kappa)\rangle_{\hat{\Sigma}_{(3,2)}} = \sum_{i=0}^{1} \varphi_1^{(i)}(0)\varphi_2^{(i)}(0) + \varphi_1(1)\varphi_2(1) + \int_0^1 \varphi_1'''(\kappa)\varphi_2'''(\kappa)d\kappa. \tag{8}$$

But in return, the RK function of $\hat{\Sigma}_{(3,2)}[0,1]$ can performs as

$$\hat{\Pi}_{\lambda}^{\{3\}}(\kappa) = \frac{1}{120}\begin{cases} \lambda\big(\mathfrak{O}_1(\kappa,\lambda) + \mathfrak{O}_2(\kappa,\lambda) + 5\mathfrak{O}_3(\kappa,\lambda)\big), & \kappa \le \lambda, \\ \kappa\big(\mathfrak{O}_1(\lambda,\kappa) + \mathfrak{O}_2(\lambda,\kappa) + 5\mathfrak{O}_3(\lambda,\kappa)\big), & \kappa > \lambda, \end{cases} \tag{9}$$

whereas $\mathfrak{O}_1(x,y)$, $\mathfrak{O}_1(x,y)$, and $\mathfrak{O}_1(x,y)$ are formulated, simultaneously, as

$$\begin{aligned} &\mathfrak{O}_1(\kappa,\lambda) = \kappa^2\lambda(6 + 120 - \kappa^3 - \lambda^3), \\ &\mathfrak{O}_2(\kappa,\lambda) = \lambda(\lambda^3 - 10\kappa^3) - 5\kappa(-24 + \lambda^3), \\ &\mathfrak{O}_3(\kappa,\lambda) = \kappa\big(\lambda(\kappa^3 - 24) + \kappa(\lambda^3 - 24)\big). \end{aligned} \tag{10}$$

To fitting adequate spaces contains the suggested solution of (1-3); a couple HSs and RK functions are setting up. Hither, we will write $\mathrm{I} = [0,1] \otimes [0,1]$ and $\|\phi\|_{\zeta}^2 = \langle \phi(\xi,\varsigma), \phi(\xi,\varsigma)\rangle_{\zeta}$, whereas $\phi \in \zeta$, $\xi, \varsigma \in \mathrm{I}$ and $\zeta \in \{\Upsilon, \hat{\Upsilon}\}$. In addendum, we will assume that $\partial_{\kappa}^3\partial_{\tau}^3\phi, \partial_{\kappa}\partial_{\tau}\phi \in L^2(\mathrm{I})$, whilst, $C(\mathrm{I})$ denotes the set of continuous functions on I.

Definition 1 The elements in $\Upsilon(\mathrm{I})$ are explored as

$$\Upsilon(\mathrm{I}) = \{\phi: \partial_{\kappa}^2\partial_{\tau}^2\phi(\kappa,\tau) \in C(\mathrm{I}) \wedge \phi(\kappa,0) = \partial_{\tau}\phi(\kappa,0) = \phi(0,\tau) = \phi(1,\tau) = 0\}, \tag{11}$$

and equipped with the inner representation product

$$\begin{aligned} \langle \phi_1(\kappa,\tau), \phi_2(\kappa,\tau)\rangle_{\Upsilon} = &\sum_{j=0}^{2} \langle \partial_{\tau}^j\phi_1(\kappa,0), \partial_{\tau}^j\phi_2(\kappa,0)\rangle_{\hat{\Sigma}_{(3,2)}} \\ &+ \int_0^1 \left[\sum_{j=0}^{1} \partial_{\tau}^2\,\partial_{\kappa}^j\phi_1(0,\tau)\partial_{\tau}^2\partial_{\kappa}^j\phi_2(0,\tau) + \partial_{\tau}^2\phi_1(1,\tau)\,\partial_{\tau}^2\phi_2(1,\tau)\right]d\tau \\ &+ \int_0^1\int_0^1 \partial_{\kappa}^3\,\partial_{\tau}^2\phi_1(\kappa,\tau)\,\partial_{\kappa}^3\,\partial_{\tau}^2\phi_2(\kappa,\tau)dxd\tau. \end{aligned} \tag{12}$$

Theorem 1 The RK function of $\Upsilon(\mathrm{I})$ can performs as

$$\mathrm{P}_{(y,s)}(\kappa,\tau)=\widehat{\Pi}_{\lambda}^{\{3\}}(\kappa)\Pi_{\varsigma}^{\{3\}}(\tau), \tag{13}$$

whereas for each $\phi(\kappa,\tau)\in\Upsilon(\mathrm{I})$, one has $\left\langle\phi(\kappa,\tau),\mathrm{P}_{(\lambda,\varsigma)}(\kappa,\tau)\right\rangle_{\Upsilon}=\phi(\lambda,\varsigma)$ and $\mathrm{P}_{(\lambda,\varsigma)}(\kappa,\tau)=\mathrm{P}_{(\kappa,\tau)}(\lambda,\varsigma)$.

Proof. From the functional framework of $\widehat{\Sigma}_{(3,2)}\,[0,1]$ and $\Sigma_{(3,2)}[0,1]$ with differentials $d\kappa$ and $d\tau$, one has

$$\begin{aligned}
&\langle\phi(\kappa,\tau),\widehat{\Pi}_{\lambda}^{\{3\}}(\kappa)\Pi_{\varsigma}^{\{3\}}(\tau)\rangle_{\Upsilon}\\
&\quad=\sum_{j=0}^{2}\langle\partial_{\tau}^{j}\phi(\kappa,0),\partial_{\tau}^{j}\widehat{\Pi}_{\lambda}^{\{3\}}(\kappa)\Pi_{\varsigma}^{\{3\}}(0)\rangle_{\widehat{\Sigma}_{(3,2)}}\\
&\quad+\int_{0}^{1}\left[\sum_{j=0}^{1}\partial_{\tau}^{2}\partial_{\kappa}^{j}\phi(0,\tau)\partial_{\tau}^{2}\partial_{\kappa}^{j}\widehat{\Pi}_{\lambda}^{\{3\}}(0)\Pi_{\varsigma}^{\{3\}}(\tau)+\partial_{\tau}^{2}\phi(1,\tau)\partial_{\tau}^{2}\widehat{\Pi}_{\lambda}^{\{3\}}(1)\Pi_{\varsigma}^{\{3\}}(\tau)\right]d\tau\\
&\quad+\int_{0}^{1}\int_{0}^{1}\partial_{\kappa}^{3}\partial_{\tau}^{2}\phi(\kappa,\tau)\partial_{\kappa}^{3}\partial_{\tau}^{2}\widehat{\Pi}_{\lambda}^{\{3\}}(\kappa)\Pi_{\varsigma}^{\{3\}}(\tau)\,d\kappa d\tau\\
&\quad=\sum_{j=0}^{2}\langle\partial_{\tau}^{j}\phi(\kappa,0),\widehat{\Pi}_{\lambda}^{\{3\}}(\kappa)\,\partial_{\tau}^{j}\Pi_{\varsigma}^{\{3\}}(0)\rangle_{\widehat{\Sigma}_{(3,2)}}\\
&\quad+\int_{0}^{1}\left[\sum_{j=0}^{1}\partial_{\tau}^{2}\partial_{\kappa}^{j}\phi(0,\tau)\partial_{\tau}^{2}\Pi_{\varsigma}^{\{3\}}(\tau)\partial_{\kappa}^{j}\widehat{\Pi}_{\lambda}^{\{3\}}(0)+\partial_{\tau}^{2}\phi(1,\tau)\widehat{\Pi}_{\lambda}^{\{3\}}(1)\partial_{\tau}^{2}\Pi_{\varsigma}^{\{3\}}(\tau)\right]d\tau\\
&\quad+\int_{0}^{1}\int_{0}^{L}\partial_{\kappa}^{3}\,\partial_{\tau}^{2}\phi(\kappa,\tau)\,\partial_{\kappa}^{3}\widehat{\Pi}_{\lambda}^{\{3\}}(\kappa)\,\partial_{\tau}^{2}\Pi_{\varsigma}^{\{3\}}(\tau)d\kappa d\tau\\
&\quad=\sum_{j=0}^{2}\partial_{\tau}^{j}\langle\phi(\kappa,0),\widehat{\Pi}_{\lambda}^{\{3\}}(\kappa)\rangle_{\widehat{\Sigma}_{(3,2)}}\,\partial_{\tau}^{j}\Pi_{\varsigma}^{\{3\}}(0)\\
&\quad+\int_{0}^{1}\partial_{\tau}^{2}\Pi_{\varsigma}^{\{3\}}(\tau)\partial_{\tau}^{2}\left[\sum_{j=0}^{1}\partial_{\kappa}^{j}\phi(0,\tau)\partial_{\kappa}^{j}\widehat{\Pi}_{\lambda}^{\{3\}}(0)+\phi(1,\tau)\widehat{\Pi}_{\lambda}^{\{3\}}(1)+\int_{0}^{1}\partial_{\kappa}^{3}\phi(\kappa,\tau)\partial_{\kappa}^{3}\widehat{\Pi}_{\lambda}^{\{3\}}(\kappa)d\kappa\right]d\tau\\
&\quad=\sum_{j=0}^{2}\partial_{\tau}^{j}\phi(\lambda,0)\,\partial_{\tau}^{j}\Pi_{\varsigma}^{\{3\}}(0)+\int_{0}^{1}\partial_{\tau}^{2}\Pi_{\varsigma}^{\{3\}}(\tau)\,\partial_{\tau}^{2}\langle\phi(\kappa,\tau),\widehat{\Pi}_{\lambda}^{\{3\}}(\kappa)\rangle_{\widehat{\Sigma}_{(3,2)}}d\tau\\
&\quad=\sum_{j=0}^{2}\partial_{\tau}^{j}\phi(\lambda,0)\,\partial_{\tau}^{j}\Pi_{\varsigma}^{\{3\}}(0)+\int_{0}^{1}\partial_{\tau}^{2}\Pi_{\varsigma}^{\{3\}}(\tau)\,\partial_{\tau}^{2}\phi(\lambda,\tau)d\tau\\
&\quad=\langle\phi(\lambda,\tau),\Pi_{\varsigma}^{\{3\}}(\tau)\rangle_{\widehat{\Sigma}_{(3,2)}}\\
&\quad=\phi(\lambda,\varsigma).
\end{aligned} \tag{14}$$

Thereafter, $\left\langle\phi(\kappa,\tau),\mathrm{P}_{(\lambda,\varsigma)}(\kappa,\tau)\right\rangle_{\Upsilon}=\phi(\lambda,\varsigma)$, while in return, $\mathrm{P}_{(\lambda,\varsigma)}(\kappa,\tau)=\left\langle\mathrm{P}_{(\lambda,\varsigma)}(\xi,\zeta),\mathrm{P}_{(\kappa,\tau)}(\xi,\zeta)\right\rangle_{\Upsilon}=\left\langle\mathrm{P}_{(\kappa,\tau)}(\xi,\zeta),\mathrm{P}_{(\lambda,\varsigma)}(\xi,\zeta)\right\rangle_{\Upsilon}=\mathrm{P}_{(\kappa,\tau)}(\lambda,\varsigma)$. ■

Definition 2 The elements in $\widehat{\Upsilon}(\mathrm{I})$ are explored as $\widehat{\Upsilon}(\mathrm{I})=\{\phi:\phi\in C(\mathrm{I})\}$ and equipped with the inner representation product

$$\begin{aligned}
\langle\phi_1(\kappa,\tau),\phi_2(\kappa,\tau)\rangle_{\widehat{\Upsilon}}&=\langle\phi_1(\kappa,0),\phi_2(\kappa,0)\rangle_{\widehat{\Sigma}_{(1,2)}}\\
&+\int_{0}^{1}\partial_{\tau}\phi_1(0,\tau)\,\partial_{\tau}\phi_2(0,\tau)d\tau+\int_{0}^{1}\int_{0}^{1}\partial_{\kappa\tau}^{2}\phi_1(\kappa,\tau)\,\partial_{\kappa\tau}^{2}\phi_2(\kappa,\tau)d\kappa d\tau.
\end{aligned} \tag{15}$$

Theorem 2 The RK function of $\widehat{\Upsilon}(\mathrm{I})$ can performs as

$$\widehat{\mathrm{P}}_{(\lambda,\varsigma)}(\kappa,\tau)=\widehat{\Pi}_{\lambda}^{\{1\}}(\kappa)\Pi_{\varsigma}^{\{1\}}(\tau), \tag{16}$$

whereas for each $\phi(\kappa,\tau)\in\widehat{\Upsilon}(\mathrm{I})$, we have $\left\langle \phi(\kappa,\tau),\hat{\mathrm{P}}_{(\lambda,\varsigma)}(\kappa,\tau)\right\rangle_{\widehat{\Upsilon}}=\phi(\lambda,\varsigma)$ and $\hat{\mathrm{P}}_{(\lambda,\varsigma)}(\kappa,\tau)=\hat{\mathrm{P}}_{(\kappa,\tau)}(\lambda,\varsigma)$.

Proof. Leaves to the reader to complete it. ■

3 TFSGM: preparation and processing

In the utilized work, the determinant function $\phi(\kappa,\tau)$ is specified whereas the TFBM (1-3) is unruffled hold. To do this fully, problem initialization for the RKHA of finding n-term pointwise numerical solution in its discrete horizon, and the construction of the orthogonal function systems of $\Upsilon(\mathrm{I})$ are utilized. In addendum, we will offering that $\{\theta_i(\kappa,\tau)\}_{i=1}^{\infty}$ is complete, whilst, $\left\{\mathrm{P}_{(\kappa_i,\tau_i)}(\kappa,\tau)\right\}_{i=1}^{\infty}$ is a linearly independent on $\Upsilon(\mathrm{I})$ in the zone that $\{(\kappa_i,\tau_i)\}_{i=1}^{\infty}$ is dense on I.

Our subsequent step is to work on vanishinization the DBC in (2) to put ϕ in $\Upsilon(\mathrm{I})$. Anyhow, the subsequent initialization could be making use of taking into account $\chi_1(0)\neq 0$. In this direction, set

$$\begin{aligned}\phi(\kappa,\tau):=\phi(\kappa,\tau)&-\tau\big(\varphi_2(\kappa)+\chi_1^{-1}(0)(\kappa-1)\varphi_1(\kappa)\varphi_2(0)-\kappa\varphi_2(1)\big)+\chi_1^{-1}(0)(\kappa-1)\varphi_1(\kappa)\chi_1(\tau)\\&-\kappa\chi_2(\tau)-\kappa\varphi_1(\kappa)+\kappa\chi_2(0).\end{aligned}\tag{17}$$

Despite the whole thing and for plainness, we will indicate the new transformed solution by $\phi(\kappa,\tau)$ in the flesh, so, we acknowledge and fixe that

$$\begin{cases}\Phi[\phi](\kappa,\tau)=\partial_\tau^{\omega}\phi(\kappa,\tau)+\mathcal{A}\,\partial_\tau\phi(\kappa,\tau)-\mathcal{B}\,\partial_\kappa^2\phi(\kappa,\tau),\\ \mathcal{H}\big(\kappa,\tau,\phi(\kappa,\tau)\big)=\hat{\psi}(\kappa,\tau)-\upsilon(\kappa,\tau)\sin\big(\phi(\kappa,\tau)\big).\end{cases}\tag{18}$$

regarding the homogenized DBC

$$\begin{cases}\phi(\kappa,0)=0,\\ \partial_\tau\phi(\kappa,0)=0,\\ \phi(0,\tau)=0,\\ \phi(1,\tau)=0.\end{cases}\tag{19}$$

For the attitude of the RKHA procedure, we realize the differential linear operator Φ and its mapping as

$$\begin{cases}\Phi\colon\Upsilon(\mathrm{I})\to\widehat{\Upsilon}(\mathrm{I}),\\ \Phi[\phi](\kappa,\tau)=\mathcal{H}\big(\kappa,\tau,\phi(\kappa,\tau)\big).\end{cases}\tag{20}$$

To texture the orthogonal function systems of $\Upsilon(\mathrm{I})$, we nominate a countable dense subset $\{(\kappa_i,\tau_i)\}_{i=1}^{\infty}$ within I. Insert $\delta_i(\kappa,\tau)=\hat{\mathrm{P}}_{(x_i,t_i)}(\kappa,\tau)$ and $\theta_i(\kappa,\tau)=\Phi^*[\delta_i](\kappa,\tau)$, whereas $\Phi^*\colon\widehat{\Upsilon}(\mathrm{I})\to\Upsilon(\mathrm{I})$. The normalized orthonormal function of $\left\{\overline{\theta}_i(\kappa,\tau)\right\}_{i=1}^{\infty}$ systems related to $\widehat{\Upsilon}(\mathrm{I})$ is commonly initialized from the execution of the Gram-Schmidt orthogonalization of $\{\theta_i(\kappa,\tau)\}_{i=1}^{\infty}$ as

$$\overline{\theta}_i(\kappa,\tau)=\sum_{k=1}^{i}\sigma_{ik}\theta_k(\kappa,\tau).\tag{21}$$

Fundamentally, the recipients should know that the use of Schwarz inequality on $\Phi\colon\Upsilon(\mathrm{I})\to\widehat{\Upsilon}(\mathrm{I})$ produce its boundedness; this intend that $\|\Phi[\phi](\kappa,\tau)\|_{\Upsilon}^2\leq C\|\phi\|_{\widehat{\Upsilon}}^2$ with $C>0$. For more clarifications see the proof of the allocated details in [30].

Theorem 3 $\{\theta_i(\kappa,\tau)\}_{i=1}^{\infty}$ is a complete in $\Upsilon(\mathrm{I})$ whereas

$$\theta_i(\kappa,\tau)=\Phi_{(\lambda,\varsigma)}[\mathrm{P}](\kappa,\tau)\big|_{(\lambda,\varsigma)=(\kappa_i,\tau_i)}.\tag{22}$$

Proof. Note that $\Phi_{(\lambda,\varsigma)}$ tick that Φ design to a function of (λ,ς). But in fact,

$$\begin{aligned}\theta_i(\kappa,\tau)&=\Phi^*[\delta_i](\kappa,\tau)\\&=\left\langle\Phi^*[\delta_i](\lambda,\varsigma),\mathrm{P}_{(\kappa,\tau)}(\lambda,\varsigma)\right\rangle_{\Upsilon}\\&=\left\langle\delta_i(\lambda,\varsigma),\Phi_{(\lambda,\varsigma)}\big[\mathrm{P}_{(\kappa,\tau)}\big](\lambda,\varsigma)\right\rangle_{\widehat{\Upsilon}}\\&=\Phi_{(\lambda,\varsigma)}\big[\mathrm{P}_{(\kappa,\tau)}\big](\lambda,\varsigma)\big|_{(\lambda,\varsigma)=(\kappa_i,\tau_i)}\\&=\Phi_{(\lambda,\varsigma)}\big[\mathrm{P}_{(\lambda,\varsigma)}\big](\kappa,\tau)\big|_{(\lambda,\varsigma)=(\kappa_i,\tau_i)}.\\&\in\Upsilon(\mathrm{I}).\end{aligned}\tag{23}$$

To complete, for each $\phi\in\Upsilon(\mathrm{I})$, pick $\langle\phi(\kappa,\tau),\theta_i(\kappa,\tau)\rangle_{\Upsilon}=0$, $i=1,2,\ldots$. Then

$$\begin{aligned}\langle \phi(\kappa,\tau),\theta_i(\kappa,\tau)\rangle_{\mathrm{N}} &= \langle \phi(\kappa,\tau),\Phi^{*}[\delta_i](\kappa,\tau)\rangle_{\Upsilon}\\ &= \langle \Phi[\phi](\kappa,\tau),\delta_i(\tau)\rangle_{\hat{\Upsilon}}\\ &= \Phi[\phi](\kappa_i,\tau_i)\\ &= 0.\end{aligned} \tag{24}$$

for $\{(\kappa_i,\tau_i)\}_{i=1}^{\infty}$ is dense on I, we get $\Phi[\phi](\kappa,\tau)=0$ via the existence of Φ^{-1}. Thus $\rho=0$. ■

Theorem 4 $\left\{\mathrm{P}_{(\kappa_i,\tau_i)}(\kappa,\tau)\right\}_{i=1}^{\infty}$ is a linearly independent on $\Upsilon(\mathrm{I})$.

Proof. Frankly, this is being demonstrated with $\left\{\mathrm{P}_{(\kappa_i,\tau_i)}(\kappa,\tau)\right\}_{i=1}^{\eta}$ is a linearly independent for each $\eta-1\geq 0$. But in return, if $\{a_i\}_{i=1}^{\eta}$ fulfill $\sum_{i=1}^{\eta}a_i\mathrm{P}_{(\kappa_i,\tau_i)}(\kappa,\tau)=0$ and taking $b_k(\kappa,\tau)\in\Upsilon(\mathrm{I})$ with $b_k(\kappa_l,\tau_l)=\delta_{l,k}$ for $l,k,1,2,\cdots,\eta$, then

$$\begin{aligned}0 &= \left\langle b_k(\kappa,\tau),\sum_{i=1}^{\eta}a_i\mathrm{P}_{(\kappa_i,\tau_i)}(\kappa,\tau)\right\rangle_{\Upsilon}\\ &= \sum_{i=1}^{\eta}a_i\left\langle b_k(\kappa,\tau),\mathrm{P}_{(\kappa_i,\tau_i)}(\kappa,\tau)\right\rangle_{\Upsilon}\\ &= \sum_{i=1}^{\eta}a_i b_k(\kappa_i,\tau_i)\\ &= a_k.\end{aligned} \tag{25}$$

Or $a_k=0$ for $k=1,2,\cdots,\eta$. ■

4 Convergence of solutions in RKHA

In this portion, functional initialization of exact and numerical pointwise solutions are given in $\Upsilon(\mathrm{I})$ depending on the Fourier expansion theorem. Over and above, convergence of $\phi_n(\kappa,\tau)\to\phi(\kappa,\tau)$ as $n\to\infty$ with some error behavior results are examined. Ultimate that, uniformly convergence of $\partial_{\kappa}^{i}\partial_{\tau}^{j}\phi_n(\kappa,\tau)\to\partial_{\kappa}^{i}\partial_{\tau}^{j}\phi(\kappa,\tau)$ with $i=0,1,2,j=0,1$ as $n\to\infty$ is offered.

Scrutinize the following qualifier: if $\phi\in C(\mathrm{I})$ and $\{\bar{\theta}_i(\kappa,\tau)\}_{i=1}^{\infty}$ an orthonormal functions system, then $\left\langle\rho(\kappa,\tau),\bar{\theta}_i(\kappa,\tau)\right\rangle_{\Upsilon}$, $i=1,2,\ldots$ is called Fourier functions of $\phi(\kappa,\tau)$ regard to $\{\bar{\theta}_i(\kappa,\tau)\}_{i=1}^{\infty}$ and $\phi(\kappa,\tau)=\sum_{i=1}^{\infty}\left\langle\phi(\kappa,\tau),\bar{\theta}_i(\kappa,\tau)\right\rangle_{\Upsilon}\bar{\theta}_i(\kappa,\tau)$ called its Fourier expansion. Anyhow, all of this qualifies us to write the subsequent outcome.

Theorem 5 If $\mathcal{K}_i=\sum_{k=1}^{i}\sigma_{ik}\Gamma\left(\kappa_k,\tau_k,\phi(\kappa_k,\tau_k)\right)$ and $\phi(\kappa,\tau)$ is the exact solution of (20) regarding to (19), then

$$\phi(\kappa,\tau)=\sum_{i=1}^{\infty}\mathcal{K}_i\bar{\theta}_i(\kappa,\tau). \tag{26}$$

Proof. Mainly, $\langle\phi(\kappa,\tau),\varphi_i(\kappa,\tau)\rangle_{\Upsilon}=\phi(x_i,t_i)$ and $\sum_{i=1}^{\infty}\mathcal{K}_i\bar{\theta}_i(\kappa,\tau)$ is the Fourier expansion on $\left\{\overline{\theta}_i(\kappa,\tau)\right\}_{i=1}^{\infty}$. Thereafter, $\sum_{i=1}^{\infty}\mathcal{K}_i\bar{\theta}_i(\kappa,\tau)$ is a convergent in $\|\cdot\|_{\Upsilon}$ whereas

$$
\begin{aligned}
\phi(\kappa,\tau) &= \sum_{i=1}^{\infty} \left\langle \phi(\kappa,\tau), \bar{\theta}_i(\kappa,\tau) \right\rangle_{\Upsilon} \bar{\theta}_i(\kappa,\tau) \\
&= \sum_{i=1}^{\infty} \langle \phi(\kappa,\tau), \sum_{k=1}^{i} \sigma_{ik} \theta_k(\kappa,\tau) \rangle_{\Upsilon} \, \bar{\theta}_i(\kappa,\tau) \\
&= \sum_{i=1}^{\infty} \sum_{k=1}^{i} \sigma_{ik} \langle \phi(\kappa,\tau), \Phi^{*} \varphi_k(\kappa,\tau) \rangle_{\Upsilon} \bar{\theta}_i(\kappa,\tau) \\
&= \sum_{i=1}^{\infty} \sum_{k=1}^{i} \sigma_{ik} \left\langle \Phi\phi(\kappa,\tau), \hat{\mathrm{P}}_{(\kappa_k,\tau_k)}(\kappa,\tau) \right\rangle_{\hat{\Upsilon}} \bar{\theta}_i(\kappa,\tau) \\
&= \sum_{i=1}^{\infty} \sum_{k=1}^{i} \sigma_{ik} \Phi\phi(\kappa_k,\tau_k) \bar{\theta}_i(\kappa,\tau) \\
&= \sum_{i=1}^{\infty} \sum_{k=1}^{i} \sigma_{ik} \mathcal{H}\big(\kappa_k,\tau_k,\phi(\kappa_k,\tau_k)\big) \bar{\theta}_i(\kappa,\tau) \\
&= \sum_{i=1}^{\infty} \mathcal{K}_i \bar{\theta}_i(\kappa,\tau) \, .
\end{aligned}
\tag{27}
$$

In else words, $\sum_{i=1}^{\infty} \mathcal{K}_i \bar{\theta}_i(\kappa,\tau)$ is solely the exact solution of (20) regarding (19). ■

For pointwise numerical output, pick out $(\kappa_1,\tau_1) = (0,0)$. From (19) $\phi(\kappa_1,\tau_1)$ is known. In addendum, pick out $\phi_0(\kappa_1,\tau_1) = \phi(\kappa_1,\tau_1)$ and realize n-term pointwise numerical solution of $\phi(\kappa,\tau)$ using its related truncating issue as $\phi_n(\kappa,\tau) = \sum_{i=1}^{n} \mathcal{K}_i \bar{\theta}_i(\kappa,\tau)$. One more time, for $\Upsilon(\mathrm{I})$ is an HS one has $\sum_{i=1}^{\infty} \mathcal{K}_i \bar{\theta}_i(\kappa,\tau) < \infty$. From this point, one can pledge that $\phi_n(\kappa,\tau)$ satisfies (19). Ultimate that, to $\|\phi_n\|_{\Upsilon} < \infty$, $\{(\kappa_i,\tau_i)\}_{i=1}^{\infty}$ is dense on I, and the exact solution of (20) regarding to (19) is unique. Thereafter, pointwise numerical solution achieved $\phi_n(\kappa,\tau) \to \phi(\kappa,\tau)$ as $n \to \infty$.

Corollary 1 The n-term pointwise numerical solution of (20) regarding to (19) fulfills:

$$
\phi_n(x,t) = \sum_{i=1}^{n} \mathcal{K}_i \bar{\theta}_i(\kappa,\tau). \tag{28}
$$

Theorem 6 $\partial_{\kappa}^{i} \partial_{\tau}^{j} \hat{\phi}_n(\kappa,\tau) \to \partial_{\kappa}^{i} \partial_{\tau}^{j} \hat{\phi}(\kappa,\tau)$ with $i = 0,1,2, j = 0,1$ as $n \to \infty$ is achieved.

Proof. Regarding (26) and (28) one awards $\|\phi - \phi_n\|_{\Upsilon} \to 0$ as $n \to \infty$. Anyhow

$$
\begin{aligned}
\left|\partial_{\kappa}^{i} \partial_{\tau}^{j} \big(\phi(\kappa,\tau) - \phi_n(\kappa,\tau)\big)\right| &= \left|\left\langle \phi(y,s) - \phi_n(y,s), \partial_{\kappa}^{i} \partial_{\tau}^{j} \Phi\big[\mathrm{P}_{(\kappa,\tau)}\big](\lambda,\varsigma) \right\rangle_{\Upsilon}\right| \\
&\le \|\phi - \phi_n\|_{\Upsilon} \left\|\partial_{\kappa}^{i} \partial_{\tau}^{j} \Phi\big[\mathrm{P}_{(\kappa,\tau)}\big](\lambda,\varsigma)\right\|_{\Upsilon} \\
&\le M_{i,j} \|\phi - \phi_n\|_{\Upsilon}.
\end{aligned}
\tag{29}
$$

Or $\left|\partial_{\kappa}^{i} \partial_{\tau}^{j} \big(\phi(\kappa,\tau) - \phi_n(\kappa,\tau)\big)\right| \to 0$ as $n \to \infty$. ■

In the posterior results, $(\hbar_{\kappa},\hbar_{\tau}) = \left(\frac{1}{n-1},\frac{1}{n-1}\right)$ with $\big(\kappa_i,\tau_j\big) = \big((i-1)\hbar_{\kappa},(j-1)\hbar_{\tau}\big)$ whereas $i = 1,2,\dots,n$ and $j = 1,2,\dots,n$. Whilst, $\|\phi(\kappa,\tau)\|_{\infty} = \max_{(\kappa,\tau)\in \mathrm{I}} |\phi(\kappa,\tau)|$ and $\phi(\kappa,\tau) - \phi_n(\kappa,\tau)$ denotes to nature errors at $(\kappa,\tau) \in \mathrm{I}$ in $\Upsilon(\mathrm{I})$.

Theorem 7 Let $\phi(\kappa,\tau)$ and $\phi_n(\kappa,\tau)$ be exact and pointwise numerical solutions of (20) regarding to (19), simultaneously. Assume that $\partial_{\kappa}^{3} \partial_{\tau} \phi(\kappa,\tau), \partial_{\kappa}^{2} \partial_{\tau}^{2} \phi(\kappa,\tau) \in C(\mathrm{I})$ whereas $\|\partial_{\kappa}^{3} \partial_{\tau} \phi(\kappa,\tau)\|_{\infty}, \|\partial_{\kappa}^{2} \partial_{\tau}^{2} \phi(\kappa,\tau)\|_{\infty} < \infty$. Then a positive constant $\mathcal{C}$ exists with

$$
\|\phi(\kappa,\tau) - \phi_n(\kappa,\tau)\|_{\infty} \le \mathcal{C} \hbar_{\tau} \hbar_{\kappa}^{2} (\hbar_{\kappa} + \hbar_{\tau}). \tag{30}
$$

Proof. In $[\kappa_i,\kappa_{i+1}] \times [\tau_j,\tau_{j+1}] \subset \mathrm{I}$, one has

$$
\partial_{\kappa}^{2} \partial_{\tau} \big(\phi(\kappa,\tau) - \phi_n(\kappa,\tau)\big) = \partial_{\kappa}^{2} \partial_{\tau} \Big(\phi(\kappa,\tau) - \phi\big(\kappa_i,\tau_j\big) + \phi_n\big(\kappa_i,\tau_j\big) - \phi_n(\kappa,\tau) + \phi\big(\kappa_i,\tau_j\big) - \phi_n\big(\kappa_i,\tau_j\big)\Big). \tag{31}
$$

Extend $\partial_{\kappa}^{2} \partial_{\tau} \phi(x,t)$ around $\big(\kappa_i,\tau_j\big)$ by employing the Taylor theorem, one bring that

$$\partial_{\kappa}^{2}\,\partial_{\tau}\phi(\kappa,\tau)=\partial_{\kappa}^{2}\,\partial_{\tau}\phi\big(\kappa_i,\tau_j\big)+\left(\hbar_{\kappa}\,\partial_{\kappa}+\hbar_{\tau}\,\partial_{\tau}\right)\partial_{\kappa}^{2}\,\partial_{\tau}\phi\big(\kappa_i+\varrho\hbar_{\kappa},\tau_j+\varrho\hbar_{\tau}\big)+\cdots,\varrho\in[0,1]. \tag{32}$$

The continuation of $\partial_{\kappa}^{3}\,\partial_{\tau}\phi$ and $\partial_{\kappa}^{2}\,\partial_{\tau}^{2}\phi$ on I utilized that

$$\left\|\partial_{\kappa}^{2}\,\partial_{\tau}\left(\phi(\kappa,\tau)-\phi_n\big(\kappa_i,\tau_j\big)\right)\right\|_{\infty}=O(\hbar_{\kappa}+\hbar_{\tau}). \tag{33}$$

By a simple refinement, one can pin

$$\left|\partial_{\kappa}^{2}\,\partial_{\tau}\left(\phi_n\big(\kappa_i,\tau_j\big)-\phi_n(\kappa,\tau)\right)\right|\leq\int_{\kappa_i}^{\kappa}\left|\partial_{\kappa}^{3}\,\partial_{\tau}\,\partial_{\tau}\,\partial_{\tau}\phi_n\big(\lambda,\tau_j\big)\right|d\lambda+\int_{\tau_j}^{\tau}\left|\partial_{\kappa}^{2}\,\partial_{\varsigma}^{2}\phi_n(\kappa,\varsigma)\right|d\varsigma. \tag{34}$$

Using $\|\cdot\|_{\infty}$, it appears that

$$\left\|\partial_{\kappa}^{2}\,\partial_{\tau}\left(\phi_n\big(\kappa_i,\tau_j\big)-\phi_n(\kappa,\tau)\right)\right\|_{\infty}=O(\hbar_{\kappa}+\hbar_{\tau}). \tag{35}$$

Given arbitrary $\epsilon>0$ utilizing Theorem 6, a sufficiently large n exists with

$$\left\|\partial_{\kappa}^{2}\,\partial_{\tau}\left(\phi\big(\kappa_i,\tau_j\big)-\phi_n\big(\kappa_i,\tau_j\big)\right)\right\|_{\infty}<\epsilon. \tag{36}$$

By combining the results in (31-36) for the election value of n, we gained

$$\left\|\partial_{\kappa}^{2}\,\partial_{\tau}\big(\phi(\kappa,\tau)-\phi_n(\kappa,\tau)\big)\right\|_{\infty}=O(\hbar_{\kappa}+\hbar_{\tau}). \tag{37}$$

Employing integral property of functions, one can be gained

$$\partial_{\kappa\tau}^{2}\,\partial_{\kappa}\,\partial_{\tau}\big(\phi(\kappa,\tau)-\phi_n(\kappa,\tau)\big)=\partial_{\kappa\tau}^{2}\big(\phi(\kappa_i,\tau)-\phi_n(\kappa_i,\tau)\big)+\int_{\kappa_i}^{\kappa}\Big(\partial_{\lambda}^{2}\,\partial_{\tau}\big(\phi(\lambda,\tau)-\phi_n(\lambda,\tau)\big)\Big)\,d\lambda. \tag{38}$$

$$\frac{\partial}{\partial t}\big(\phi(\kappa,\tau)-\phi_n(\kappa,\tau)\big)=\partial_{\tau}\big(\phi(\kappa_i,\tau)-\phi_n(\kappa_i,\tau)\big)+\int_{\kappa_i}^{\kappa}\Big(\partial_{\lambda\tau}^{2}\big(\phi(\lambda,\tau)-\phi_n(\lambda,\tau)\big)\Big)\,d\lambda. \tag{39}$$

$$\phi(\kappa,\tau)-\phi_n(\kappa,\tau)=\phi(\kappa,\tau_i)-\phi_n(\kappa,\tau_i)+\int_{\tau_i}^{\tau}\Big(\partial_{\varsigma}\big(\phi(\kappa,\varsigma)-\phi_n(\kappa,\varsigma)\big)\Big)\,d\varsigma. \tag{40}$$

Using (37-40) and utilizing Theorem 6, one can see

$$\|\phi(\kappa,\tau)-\phi_n(\kappa,\tau)\|_{\infty}\leq\mathcal{C}(\hbar_{\tau}\hbar_{\kappa}^{3}+\hbar_{\tau}^{2}\hbar_{\kappa}^{2}). \tag{41}$$

Or $\|\phi(\kappa,\tau)-\phi_n(\kappa,\tau)\|_{\infty}\leq\mathcal{C}\hbar_{\tau}\hbar_{\kappa}^{2}(\hbar_{\kappa}+\hbar_{\tau})$ with $\mathcal{C}>0$. ■

Ultimate that, we discussed hither the behaviour of $\{\phi(\kappa,\tau)-\phi_n(\kappa,\tau)\}_{n=1}^{\infty}$ in $\|\cdot\|_{\Upsilon}$. The connection

$$\|\phi(\kappa,\tau)-\phi_n(\kappa,\tau)\|_{\Upsilon}^{2}=\sum_{i=n+1}^{\infty}\left(\sum_{k=1}^{i}\sigma_{ik}\mathcal{H}\big(\kappa_k,\tau_k,\phi(\kappa_k,\tau_k)\big)\right)^{2}, \tag{42}$$

harvest that $\{\phi(\kappa,\tau)-\phi_n(\kappa,\tau)\}_{n=1}^{\infty}\searrow$ in $\|\cdot\|_{\Upsilon}$. But as $\sum_{i=1}^{\infty}\mathcal{K}_i\bar{\theta}_i(\kappa,\tau)<\infty$, one can finds $\|\phi(\kappa,\tau)-\phi_n(\kappa,\tau)\|_{\Upsilon}^{2}\to 0$ as $n\to\infty$. This is only the proof of the following score.

Theorem 8 Let $\phi(\kappa,\tau)$ and $\phi_n(\kappa,\tau)$ be exact and pointwise numerical solutions of (20) regarding to (19), simultaneously. Then $\{\phi(\kappa,\tau)-\phi_n(\kappa,\tau)\}_{n=1}^{\infty}\searrow$ in $\|\cdot\|_{\Upsilon}$ with $\|\phi(\kappa,\tau)-\phi_n(\kappa,\tau)\|_{\Upsilon}\to 0$ as $n\to\infty$.

5 RKHA junctures and mathematical debates

The inferred scientific formalism is computationally decided not exclusively to check the theoretical declarations yet, additionally to contrast the numerical outcomes obtained and the specific arrangements recognized and to affirm the viability of the techniques utilized. To confirm the reliability and high degree of accurateness of the proposed approach, a couple of numerical applications for TFBM besides their fractional hereditary features within two geometries are performed.

5.1 RKHA phases

To use the RKHA, divide I into $p\times q$ points against $\mathrm{I}_{\kappa}=\frac{1}{p}$ and $\mathrm{I}_{\tau}=\frac{1}{q}$ whereas $p,q\in\mathbb{N}$. Anyhow the connection points (κ_l,τ_m) on I can be defined, simultaneously, as

$$(\kappa_l,\tau_m)=(l\mathrm{I}_{\kappa},m\,\mathrm{I}_{\tau}),l=0,1,2,\cdots,p,m=0,1,2,\cdots,q. \tag{43}$$

The coefficients of orthogonalization σ_{ik} in (21) are computed as the first algorithm.

Algorithm 1. Finding orthogonalization coefficients σ_{ik} of $\theta_k(\kappa,\tau)$ in $\overline{\theta}_i(\kappa,\tau)$:

Stage 1: Pick out $\mathscr{f}_{i,p}(\tau)=\left\langle \theta_i(\tau),\overline{\theta}_p(t)\right\rangle_{\mathrm{Y}}$;

Stage 2: Pick out $\mathscr{g}_i(\tau)=\|\theta_i\|_{\mathrm{Y}}^2-\sum_{p=1}^{i-1}\mathscr{f}_{i,p}^2(\tau)$;

Stage 3: For $i=2,3,\ldots$ and $k=1,2,\ldots,i$, apply

$$\begin{aligned}&\sigma_{11}=\|\theta_1\|_{\mathrm{Y}},\\&\sigma_{ii}=\frac{1}{\sqrt{\mathscr{g}_i(\tau)}},i\neq 1,\\&\sigma_{ij}=-\frac{1}{\sqrt{\mathscr{g}_i(\tau)}}\sum_{p=j}^{i-1}\mathscr{f}_{i,p}^2(\tau)\sigma_{pj},i>j.\end{aligned}\tag{44}$$

The pointwise numerical solvability of TFSGM can be accomplished by stratifying the stages in the next second algorithm.

Algorithm 2. Finding $\phi_n(\kappa_l,\tau_m)$ of $\phi(\kappa,\tau)$ in TFSGM (1-3) on $\mathcal{D}$:

Stage 1: Pick out $n=pq$ collocation points in I;

Stage 2: Pick out $i=1,2,\cdots,n$ and $k=1,2,\ldots,i$;

Stage 3: Design $\theta_i(\kappa_l,\tau_m)=\Phi_{(\lambda,\varsigma)}[\mathrm{P}](\kappa,\tau)\big|_{(\lambda,\varsigma)=(\kappa_l,\tau_m)}$;

Stage 4: Take out the orthogonalization coefficients σ_{ik};

Stage 5: Design $\overline{\theta}_i(\kappa_l,\tau_m)=\sum_{k=1}^{i}\sigma_{ik}\,\theta_i(\kappa_l,\tau_m)$;

Stage 6: Pick $\phi_0(\kappa_1,\tau_1)$;

Stage 7: Design $i=1$;

Stage 8: Design $\mathcal{K}_i=\sum_{k=1}^{i}\sigma_{ik}\,\mathcal{H}(\kappa_l,\tau_m)$;

Stage 9: Design $\phi_i(\kappa_l,\tau_m)=\sum_{k=1}^{i}\mathcal{K}_i\overline{\theta}_k(\kappa_l,\tau_m)$;

Stage 10: If $i<n$, then design $i=i+1$ and seek 8, else stop.

5.2 Couple applications on TFSGM

In all started, invoke that $\mathrm{I}_\kappa=\frac{1}{p}$ in [0,1] and $\mathrm{I}_\tau=\frac{1}{q}$ in [0,1] whereas $(\kappa_l,\tau_m)=lm\mathrm{I}_\kappa\mathrm{I}_\tau$. Again, invoke from (3) $\partial_\tau^\omega\phi(\kappa,\tau)=\Gamma^{-1}(2-\omega)\int_0^\tau(t-\omega)^{1-\alpha}\,\partial_t^2\phi(\kappa,t)dt$ is the CTFPD over the measurement interval $0\leq t<\tau\leq 1$ and $1<\omega<2$ and not deny to use Algorithms 1 and 2.

Application 1: Primarily, look for the TFSGM of the pattern:

$$\partial_\tau^\omega\phi(\kappa,\tau)+\partial_\tau\phi(\kappa,\tau)-\partial_\kappa^2\phi(\kappa,\tau)+\exp(-\kappa^2)\sin\big(\phi(\kappa,\tau)\big)=\psi(\kappa,\tau),\tag{45}$$

regarding the DBC

$$\begin{cases}\phi(\kappa,0)=0,\\ \partial_\tau\phi(\kappa,0)=0,\\ \phi(0,\tau)=0,\\ \phi(1,\tau)=\exp(-1)\,\tau^{2+\alpha}.\end{cases}\tag{46}$$

Hither, $(\kappa,\tau)\in\Omega$ and $1<\omega<2$ provided that the variable source term function $\psi(\kappa,\tau)$ is fixed such as the source term function $\phi(\kappa,\tau)$ is

$$\phi(\kappa,\tau)=\kappa\exp(-\kappa^2)\,\tau^{2+\alpha}.\tag{47}$$

Application 2: Anew, look for the TFSGM of the pattern:

$$\partial_\tau^\omega\phi(\kappa,\tau)+\partial_\tau\phi(\kappa,\tau)-2\,\partial_\kappa^2\phi(\kappa,\tau)+(\cos(\kappa^2)+\sin(\kappa^2))\sin\big(\phi(\kappa,\tau)\big)=\psi(\kappa,\tau),\tag{48}$$

regarding the DBC

$$\begin{cases} \phi(\kappa,0)=0, \\ \partial_\tau \phi(\kappa,0)=0, \\ \phi(0,\tau)=\tau^{2+\alpha}, \\ \phi(1,\tau)=\cos(1)\,\tau^{2+\alpha}+\sin(1)\,\tau^{2\alpha}. \end{cases} \tag{49}$$

Hither, $(\kappa,\tau)\in\Omega$ and $1<\omega<2$ provided that the variable source term function $\psi(\kappa,\tau)$ is fixed such as the source term function $\phi(\kappa,\tau)$ is

$$\phi(\kappa,\tau)=\cos(\kappa^2)\,\tau^{2+\alpha}+\sin(\kappa^2)\,\tau^{2\alpha}. \tag{50}$$

5.3 Tabulation debates

The pointwise numerical solution of the TFSGM in the CTFPD sense is worthy for foreseeing the dynamic attitudes of several physical and engineering models, inclusive heat conduction, quantum chemistry, diffusion process, and mechanical models. Closest, tabulated results outcomes in discrete issues and short debates are discussed and utilized to assure both theoretical framework and RKHA.

Following, numerical pointwise effectiveness of (κ_l,τ_m) will be offered for Applications (1-2) as next:

- Tables (1-4) relates to Application 1 and tabulates $|\phi(\kappa_l,\tau_m)-\phi_n(\kappa_l,\tau_m)|$ for pointwise numerically approximating the source term function $\phi(\kappa_l,\tau_m)$ with $\omega\in\{2,1.75,1.5,1.25\}$ over Ω.
- Tables (5-8) relates to Application 2 and tabulates $|\phi(\kappa_l,\tau_m)-\phi_n(\kappa_l,\tau_m)|$ for pointwise numerically approximating the source term function $\phi(\kappa_l,\tau_m)$ with $\omega\in\{2,1.75,1.5,1.25\}$ over Ω.

Table 1: Pointwise numerical outcomes for state variable $\phi_n(\kappa_l,\tau_m)$ in Application 1 over Ω with $\omega=2$.

κ_l/τ_m	0	0.2	0.4	0.6	0.8	1
0	0	0	0	0	0	0
0.2	0	1.02×10^{-4}	5.76×10^{-5}	3.98×10^{-4}	2.47×10^{-4}	6.91×10^{-5}
0.4	0	9.06×10^{-5}	5.37×10^{-5}	7.76×10^{-5}	5.59×10^{-5}	6.50×10^{-5}
0.6	0	8.14×10^{-5}	5.02×10^{-5}	2.98×10^{-4}	6.93×10^{-5}	6.04×10^{-5}
0.8	0	7.38×10^{-5}	4.72×10^{-5}	5.87×10^{-5}	7.48×10^{-5}	5.71×10^{-5}
1	0	0	0	0	0	0

Table 2: Pointwise numerical outcomes for state variable $\phi_n(\kappa_l,\tau_m)$ in Application 1 over Ω with $\omega=1.75$.

κ_l/τ_m	0	0.2	0.4	0.6	0.8	1
0	0	0	0	0	0	0
0.2	0	4.27×10^{-4}	4.81×10^{-4}	2.93×10^{-4}	2.09×10^{-4}	4.66×10^{-4}
0.4	0	3.72×10^{-4}	1.33×10^{-4}	2.74×10^{-4}	2.03×10^{-4}	5.72×10^{-5}
0.6	0	6.88×10^{-5}	2.62×10^{-4}	2.57×10^{-4}	1.11×10^{-4}	5.22×10^{-5}
0.8	0	3.96×10^{-4}	3.68×10^{-4}	2.43×10^{-4}	1.04×10^{-4}	4.66×10^{-4}
1	0	0	0	0	0	0

Table 3: Pointwise numerical outcomes for state variable $\phi_n(\kappa_l,\tau_m)$ in Application 1 over Ω with $\omega=1.5$.

κ_l/τ_m	0	0.2	0.4	0.6	0.8	1
0	0	0	0	0	0	0
0.2	0	5.76×10^{-4}	4.44×10^{-4}	2.56×10^{-3}	1.12×10^{-3}	8.50×10^{-4}
0.4	0	1.62×10^{-3}	5.25×10^{-4}	1.93×10^{-3}	1.06×10^{-3}	4.10×10^{-4}
0.6	0	3.97×10^{-4}	4.42×10^{-4}	1.71×10^{-3}	1.27×10^{-3}	1.11×10^{-3}
0.8	0	2.68×10^{-3}	3.62×10^{-3}	5.41×10^{-4}	3.40×10^{-3}	7.67×10^{-4}
1	0	0	0	0	0	0

Table 4: Pointwise numerical outcomes for state variable $\phi_n(\kappa_l,\tau_m)$ in Application 1 over Ω with $\omega=1.25$.

κ_l/τ_m	0	0.2	0.4	0.6	0.8	1
0	0	0	0	0	0	0
0.2	0	3.03×10^{-3}	3.06×10^{-3}	4.81×10^{-3}	1.62×10^{-3}	7.46×10^{-3}
0.4	0	1.61×10^{-3}	5.03×10^{-3}	4.54×10^{-3}	1.40×10^{-3}	3.44×10^{-3}
0.6	0	1.41×10^{-3}	9.14×10^{-3}	3.55×10^{-3}	1.64×10^{-3}	2.35×10^{-3}
0.8	0	1.27×10^{-3}	4.05×10^{-3}	2.04×10^{-3}	1.19×10^{-3}	4.63×10^{-3}

1	0		0		0		0		0		0

Table 5: Pointwise numerical outcomes for state variable $\phi_n(\kappa_l, \tau_m)$ in Application 2 over Ω with $\omega = 2$.

κ_l/τ_m	0	0.2	0.4	0.6	0.8	1
0	0	0	0	0	0	0
0.2	0	9.19×10^{-5}	1.49×10^{-4}	6.75×10^{-5}	4.51×10^{-5}	1.34×10^{-4}
0.4	0	2.32×10^{-4}	1.26×10^{-4}	9.14×10^{-5}	4.01×10^{-5}	1.15×10^{-4}
0.6	0	3.41×10^{-5}	1.15×10^{-4}	5.17×10^{-5}	3.00×10^{-5}	1.05×10^{-4}
0.8	0	2.59×10^{-5}	5.02×10^{-5}	2.36×10^{-4}	2.41×10^{-4}	8.05×10^{-5}
1	0	0	0	0	0	0

Table 6: Pointwise numerical outcomes for state variable $\phi_n(\kappa_l, \tau_m)$ in Application 2 over Ω with $\omega = 1.75$.

κ_l/τ_m	0	0.2	0.4	0.6	0.8	1
0	0	0	0	0	0	0
0.2	0	4.37×10^{-4}	1.25×10^{-4}	1.36×10^{-4}	5.61×10^{-4}	4.29×10^{-4}
0.4	0	3.84×10^{-4}	1.71×10^{-4}	1.06×10^{-4}	6.24×10^{-4}	3.80×10^{-4}
0.6	0	2.89×10^{-4}	2.91×10^{-4}	9.57×10^{-5}	6.47×10^{-5}	3.56×10^{-4}
0.8	0	2.23×10^{-4}	7.83×10^{-5}	6.85×10^{-4}	6.02×10^{-4}	3.38×10^{-4}
1	0	0	0	0	0	0

Table 7: Pointwise numerical outcomes for state variable $\phi_n(\kappa_l, \tau_m)$ in Application 2 over Ω with $\omega = 1.5$.

κ_l/τ_m	0	0.2	0.4	0.6	0.8	1
0	0	0	0	0	0	0
0.2	0	2.51×10^{-3}	4.78×10^{-4}	2.48×10^{-3}	1.31×10^{-3}	4.88×10^{-4}
0.4	0	2.35×10^{-3}	5.48×10^{-4}	2.19×10^{-3}	1.73×10^{-3}	5.78×10^{-4}
0.6	0	2.20×10^{-3}	4.85×10^{-4}	1.25×10^{-3}	1.10×10^{-3}	4.43×10^{-3}
0.8	0	2.79×10^{-3}	3.99×10^{-3}	1.70×10^{-3}	1.01×10^{-3}	3.02×10^{-4}
1	0	0	0	0	0	0

Table 8: Pointwise numerical outcomes for state variable $\phi_n(\kappa_l, \tau_m)$ in Application 2 over Ω with $\omega = 1.25$.

κ_l/τ_m	0	0.2	0.4	0.6	0.8	1
0	0	0	0	0	0	0
0.2	0	2.13×10^{-3}	1.04×10^{-3}	8.49×10^{-3}	4.86×10^{-3}	1.93×10^{-3}
0.4	0	1.76×10^{-3}	5.48×10^{-3}	5.14×10^{-3}	4.75×10^{-3}	1.31×10^{-3}
0.6	0	1.56×10^{-3}	6.87×10^{-3}	4.09×10^{-3}	3.56×10^{-3}	1.35×10^{-3}
0.8	0	1.39×10^{-3}	9.36×10^{-3}	8.15×10^{-3}	3.01×10^{-3}	1.21×10^{-3}
1	0	0	0	0	0	0

Of the results acquired, one can be observed that perfect precisions of error estimations for pointwise numerical solutions of the source term functions $\phi(\kappa_l, \tau_m)$ are closely concerned with stuffing time as well as to order of the CTFPDs used, whereas additional precisions solutions can be acquired employing more partitions and iterations.

5.4 Graphical debates

Now, three-dimensional geometric attitudes over memory-heritage merits of the RKHA are elaborated. Closest, schematic plot outcomes are discussed and utilized to assure both theoretical framework and RKHA.

Following, pointwise numerical effectiveness of (κ_l, τ_m) will be offered for Applications (1-2) as next:

- Figure 1 (a-d) relates to Application 1 and plots $\phi_n(\kappa_l, \tau_m)$ for pointwise numerically approximating the source term function $\phi(\kappa_l, \tau_m)$ with $\omega \in \{2, 1.75, 1.5, 1.25\}$ over Ω.
- Figure 2 (a-d) relates to Application 2 and plots $\phi_n(\kappa_l, \tau_m)$ for pointwise numerically approximating the source term function $\phi(\kappa_l, \tau_m)$ with $\omega \in \{2, 1.75, 1.5, 1.25\}$ over Ω.

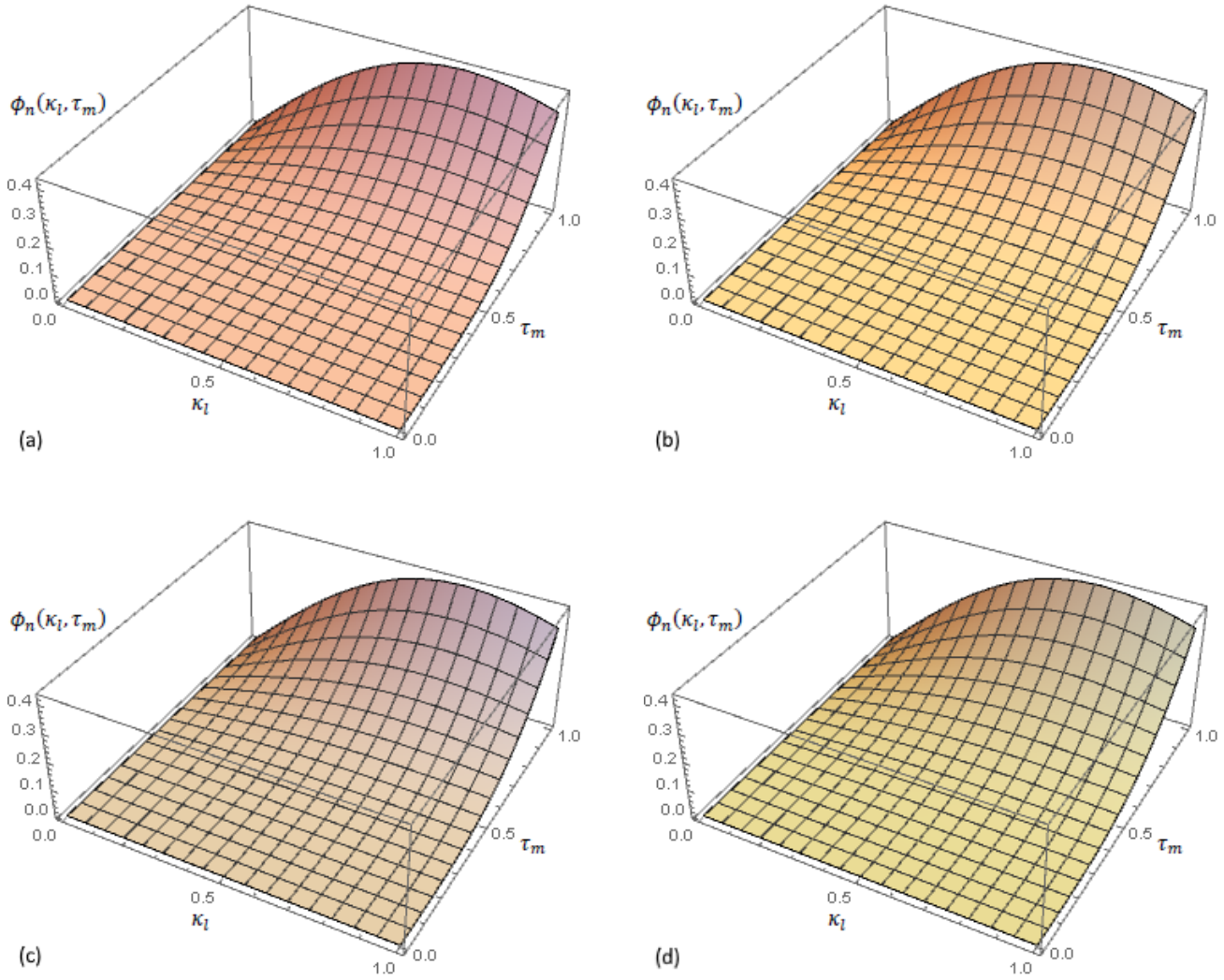

Figure 1: The 3D plots of pointwise numerical solutions of TFSGM in Application 1 on Ω: (a) $\omega = 2$, (b) $\omega = 1.75$, (c) $\omega = 1.5$, and (d) $\omega = 1.25$.

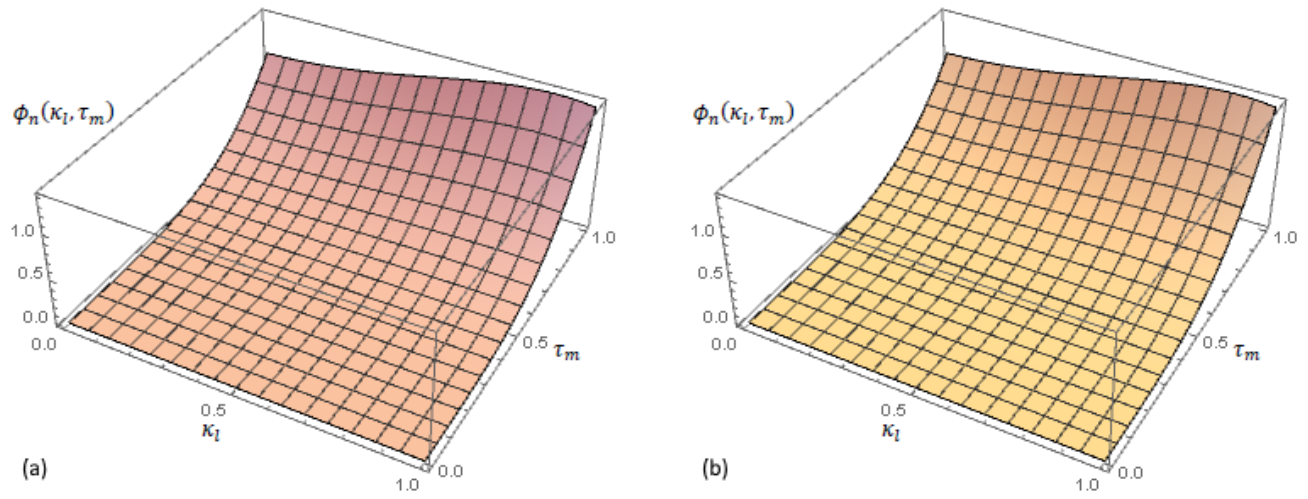

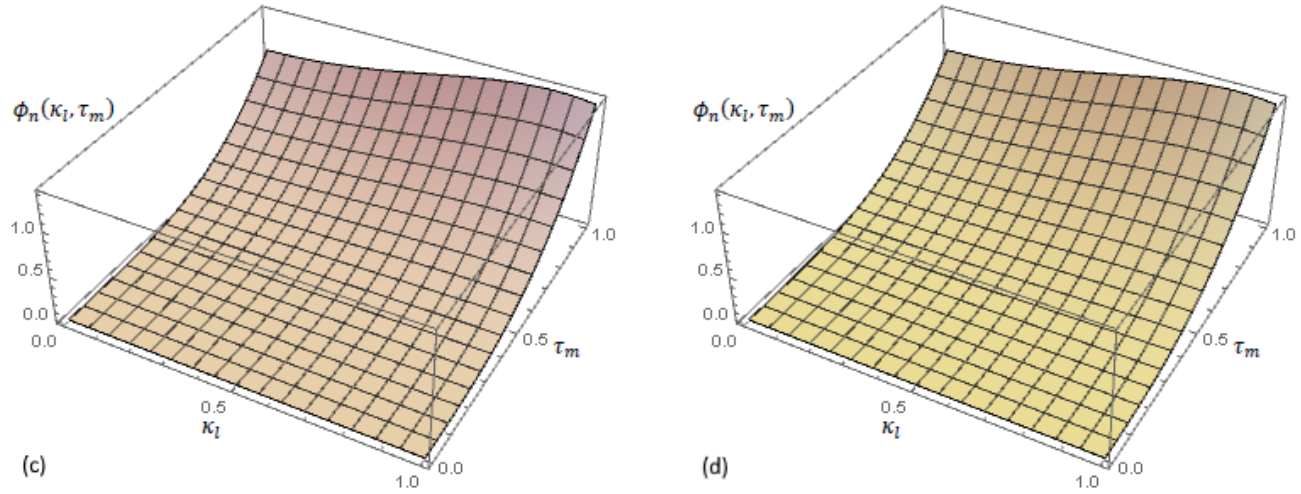

Figure 2: The 3D plots of pointwise numerical solutions of TFSGM in Application 2 on Ω: (a) $\omega = 2$, (b) $\omega = 1.75$, (c) $\omega = 1.5$, and (d) $\omega = 1.25$.

From the previous plots, one can show that all graphs are nearly matched, identical in their attitudes, and nice agreement with each other, particularly, when integer-order derivatives are considered. Indeed, the CTFPDs have strong effects on TFSGM profiles.

Following, two-dimensional geometric attitudes over memory-heritage merits of the RKHA are elaborated in terms effect of contour plots regarding κ_l and τ_m. Anyhow, pointwise numerical effectiveness plots of (κ_l, τ_m) will be offered for Applications (1-2) as next:

- Figure 3 (a-d) relates to Application 1 and utilized the contour plots for pointwise numerically approximating the source term function $\phi_n(\kappa_l, \tau_m)$ with $\omega \in \{1, 0.75, 0.5, 0.25\}$ over $[0.5,1] \times [0.5,1]$.
- Figure 4 (a-d) relates to Application 2 and utilized the contour plots for pointwise numerically approximating the source term function $\phi_n(\kappa_l, \tau_m)$ with $\omega \in \{1, 0.75, 0.5, 0.25\}$ over $[0.5,1] \times [0.5,1]$.

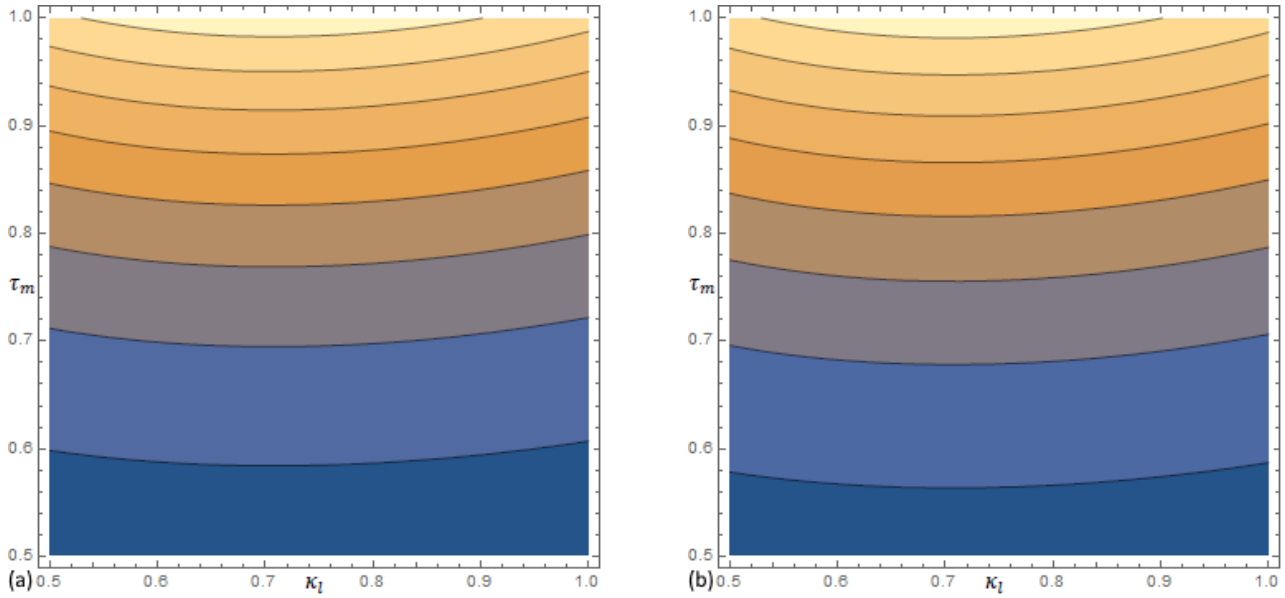

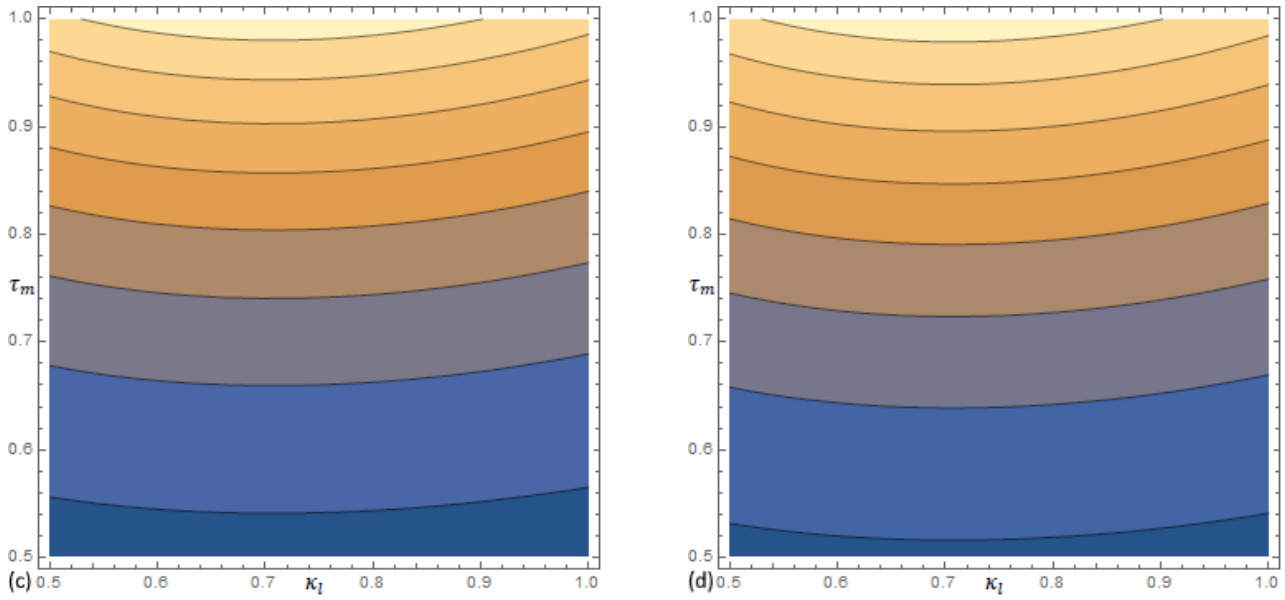

Figure 3: The 2D contour plots of pointwise numerical solutions of TFSGM in Application 1 on [0.5,1] × [0.5,1]: (a) $\omega = 2$, (b) $\omega = 1.75$, (c) $\omega = 1.5$, and (d) $\omega = 1.25$.

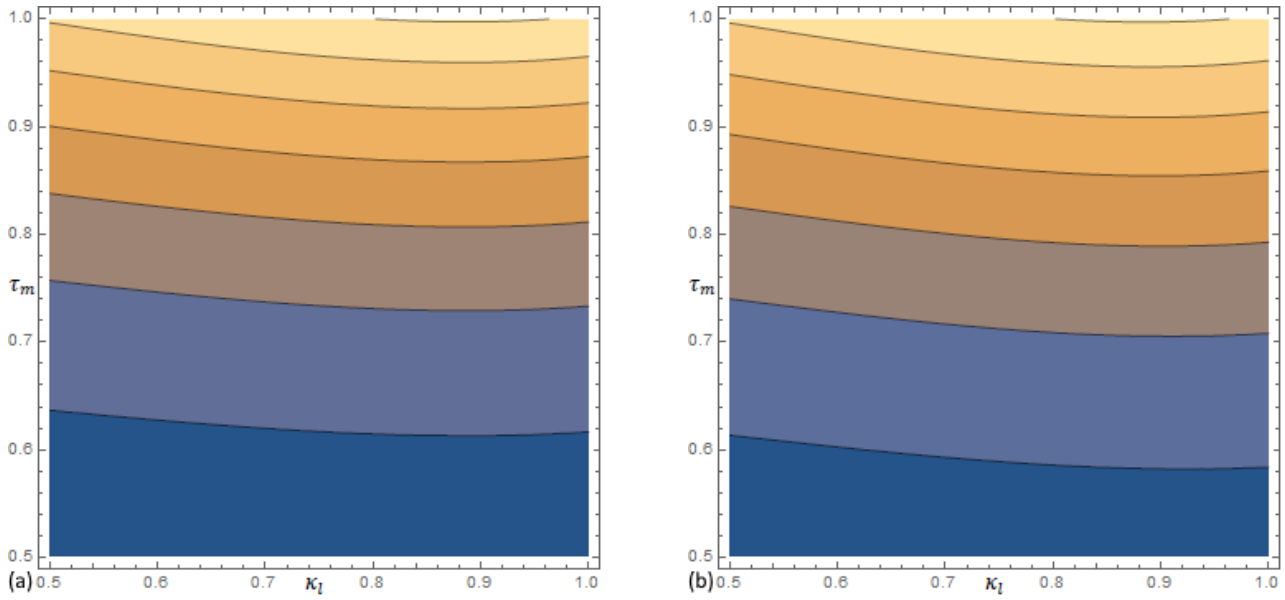

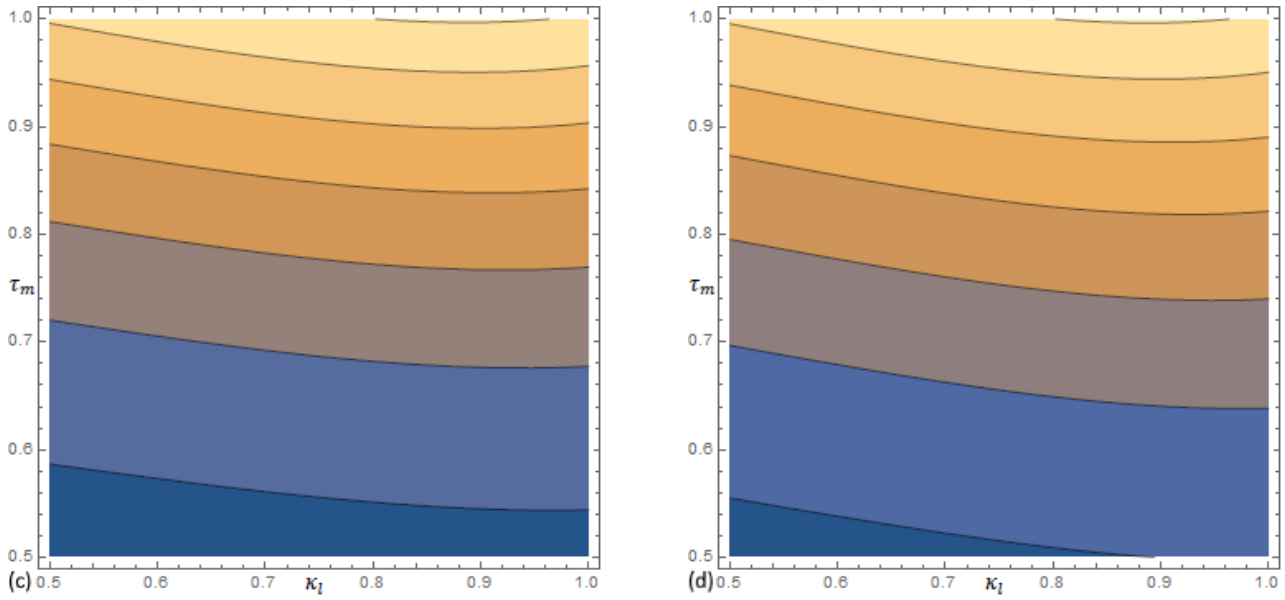

Figure 4: The 2D contour plots of pointwise numerical solutions of TFSGM in Application 2 on [0.5,1] × [0.5,1]: (a) $\omega = 2$, (b) $\omega = 1.75$, (c) $\omega = 1.5$, and (d) $\omega = 1.25$.

We point out right here that, the contour plot generates colorized grayscale output, wherein large values are shown lighter, while in return its treats κ_l and τ_m as local and effectively using block. In addendum, the contour plot computes ϕ_n only after specifying fixed values to κ_l and τ_m.

Ultimately, two-dimensional geometric attitudes over memory-heritage merits of the RKHA are elaborated in terms effect of density plots regarding κ_l and τ_m. Anyhow, pointwise numerical effectiveness plots of (κ_l, τ_m) will be offered for Applications (1-2) as next:

- Figure 5 (a-d) relates to Application 1 and utilized the density plots for pointwise numerically approximating the source term function $\phi_n(\kappa_l, \tau_m)$ with $\omega \in \{1,0.75,0.5,0.25\}$ over [0.5,1] × [0.5,1].
- Figure 6 (a-d) relates to Application 2 and utilized the density plots for pointwise numerically approximating the source term function $\phi_n(\kappa_l, \tau_m)$ with $\omega \in \{1,0.75,0.5,0.25\}$ over [0.5,1] × [0.5,1].

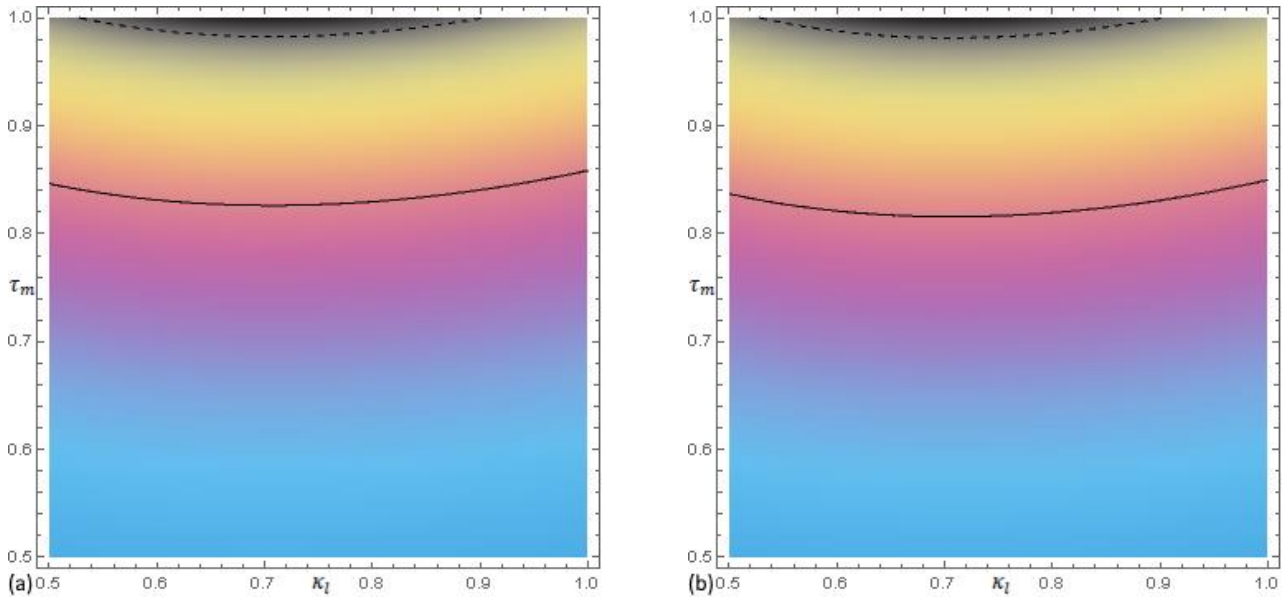

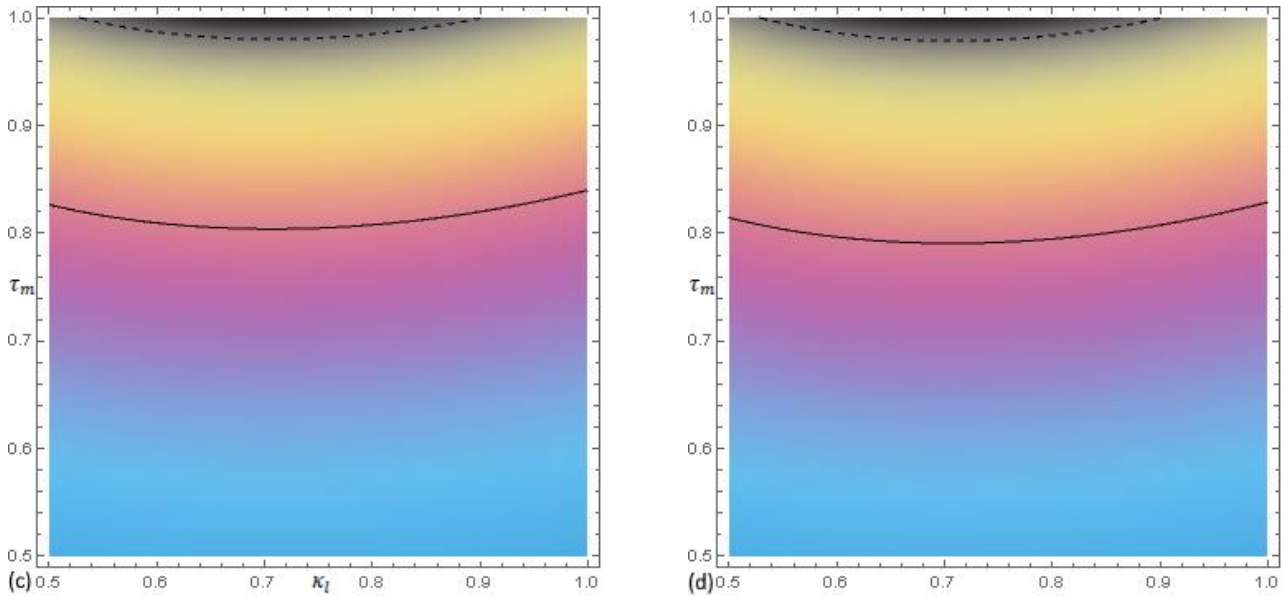

Figure 5: The 2D density plots of pointwise numerical solutions of TFSGM in Application 1 on [0.5,1] × [0.5,1]: (a) $\omega = 2$, (b) $\omega = 1.75$, (c) $\omega = 1.5$, and (d) $\omega = 1.25$.

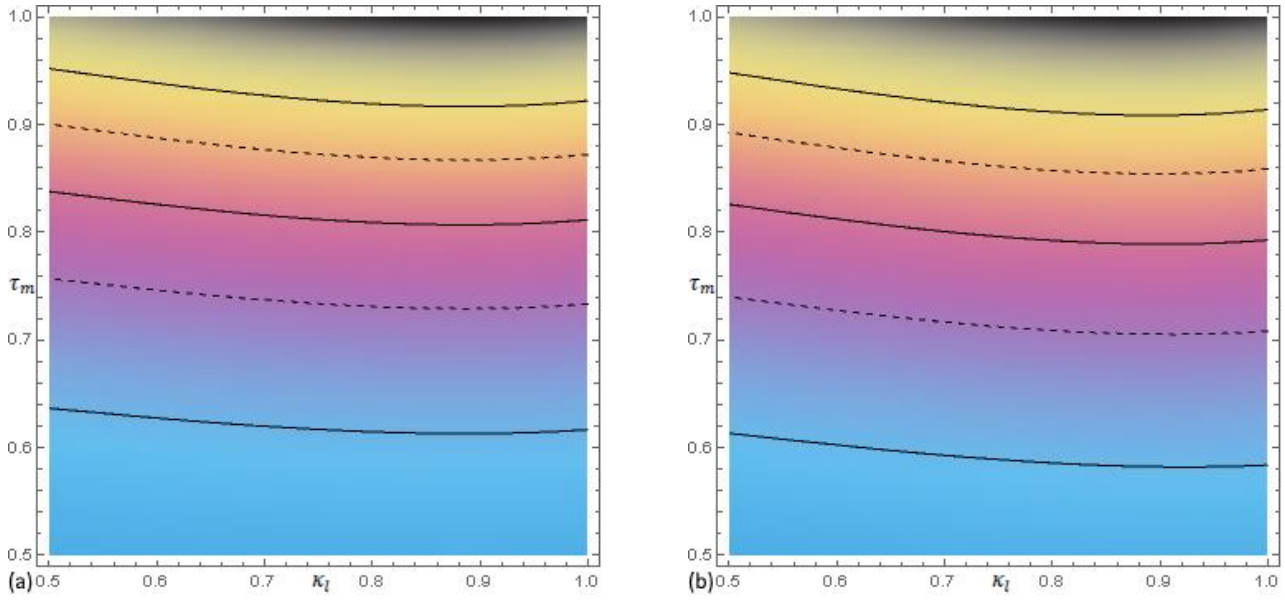

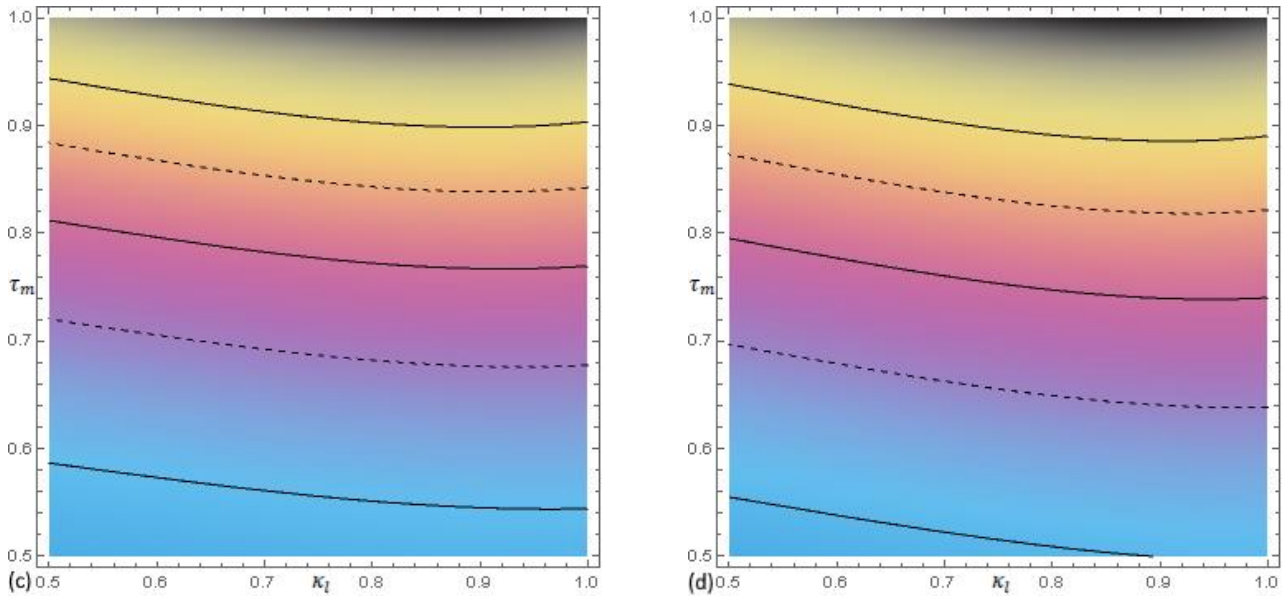

Figure 6: The 2D density plots of pointwise numerical solutions of TFSGM in Application 2 on [0.5,1] × [0.5,1]: (a) $\omega = 2$, (b) $\omega = 1.75$, (c) $\omega = 1.5$, and (d) $\omega = 1.25$.

We point out right here that, the density plot generates colorized output, wherein large values are shown lighter, while in return its treats κ_l and τ_m as local and effectively using block. In addendum, the density plot computes ϕ_n only after specifying fixed values to κ_l and τ_m.

6 Highlight, concluding, and future

This utilization and discussion goals to perform a numerical algorithm in the RK Hilbert approach to take out a pointwise numerical solution of the TFSGM regarding the DBC in which the CTFPD approach for non-integer order basis is applied. This goal has been carried out by beneficiating and extending the applications of the RKHA for treating these types of fractional models without any linearization or limitations. The most remarkable features of the RKHA are pointwise numerical solutions converge uniformly to the exact one and its partial derivatives, whilst, frame of numerical programming is natural and the computations are very swift. Utilizing this algorithm, a visible truncated sequence of $\phi_n(\kappa_l, \tau_m)$ solutions has been shown and found to converge to exact solutions uniformly in $\|\cdot\|_\Upsilon$. Ultimately, a couple of numerical trials were outrighted to advocate the potentiality and generality of the RKHA. The gained results show the full reliability and execution of such adaptation, which can be presented efficiently as a substitutional approach in solving various kinds of fractional models emerging in scientific matters. Our near-future research will focus on the solvability of TFSGM regarding the integral condition in which the CTFPD approach is used.

References

[1] M. Ablowitz, P. Clarkson, Solitons, Nolinear Volution Equations and Inverse Scattering, Cambridge University Press, UK, 1991.

[2] R. K. Dodd, J. C. Eilbeck, J. D. Gibbon, H. C. Morris, Solitons and Nonlinear Wave Equations, Academic Press, USA, 1984.

[3] F. Demengel, G. Demengel, Functional Spaces for the Theory of Elliptic Partial Differential Equations, UK, 2012.

[4] H. T. Banks, R. C. Smith, and Y. Wang, Smart Material Structures: Modeling, Estimation and Control, Research in Applied Mathematics, Wiley, USA, 1996.

[5] S. Guo, L. Mei, Y. Hou, Z. Zhang, An efficient finite difference/Hermite–Galerkin spectral method for time-fractional coupled sine–Gordon equations on multidimensional unbounded domains and its application in numerical simulations of vector solitons, Computer Physics Communications 237 (2019) 110-128.

[6] Y. Fu, W. Cai, Y. Wang, A linearly implicit structure-preserving scheme for the fractional sine-Gordon equation based on the IEQ approach, Applied Numerical Mathematics 160 (2021) 368-385.

[7] Z. Xing, L. Wen, W. Wang, An explicit fourth-order energy-preserving difference scheme for the Riesz space-fractional Sine–Gordon equations, Mathematics and Computers in Simulation 181 (2021) 624-641.
[8] H. Karayer, D. Demirhan, F. Buyukkilic, Solutions of local fractional sine-Gordon equations, Waves in Random and Complex Media 29 (2019) 227-235.
[9] A. Akgül, M. Inc, A. Kilicman, D. Baleanu, A new approach for one-dimensional sine-Gordon equation, Advances in Difference Equations (2016) 2016:8.
[10] F. Mainardi, Fractional Calculus and Waves in Linear Viscoelasticity, Imperial College Press, UK, 2010.
[11] G.M. Zaslavsky, Hamiltonian Chaos and Fractional Dynamics, Oxford University Press, UK, 2005.
[12] I. Podlubny, Fractional Differential Equations, Academic Press, USA, 1999.
[13] S.G. Samko, A.A. Kilbas, O.I. Marichev, Fractional Integrals and Derivatives Theory and Applications, Gordon and Breach, USA, 1993.
[14] A. Kilbas, H. Srivastava, J. Trujillo, Theory and Applications of Fractional Differential Equations, Elsevier, Amsterdam, Netherlands, 2006.
[15] J.L. Bona, M.E. Schonbek, Travelling-wave solutions to the Korteweg-de Vries-Burgers equation, Proceedings of the Royal Society of Edinburgh: Section A Mathematics 101 (1985) 207-226.
[16] A. Jeffrey, S. Xu, Exact solutions to the Korteweg-de Vries-Burgers equation, Wave Motion 11 (1989) 559-564.
[17] R.F. Bikbaev, Shock waves in the modified Korteweg-de Vries-Burgers equation, Journal of Nonlinear Science 5 (1995) 1-10.
[18] A. Atangana, D. Baleanu, New fractional derivatives with non-local and non-singular kernel: theory and application to heat transfer model, Thermal Science 20 (2016) 763-769.
[19] A. Atangana, J.J. Nieto, Numerical solution for the model of RLC circuit via the fractional derivative without singular kernel, Advances in Mechanical Engineering 7(2015) 1-7.
[20] A. Atangana, J.F. Gómez-Aguilar, Decolonisation of fractional calculus rules: Breaking commutativity and associativity to capture more natural phenomena, The European Physical Journal Plus 133 (2018) 1-22.
[21] A. Atangana, J.F. Gómez-Aguilar, Fractional derivatives with no-index law property: Application to chaos and statistics, Chaos Solitons & Fractals 114 (2018) 516-535.
[22] M. Senol, S. Atpinar, Z. Zararsiz, S. Salahshour, A. Ahmadian, Approximate solution of time-fractional fuzzy partial differential equations, Computational and Applied Mathematics 38 (2019) 1-18.
[23] S. Kumar, A. Kumar, B. Samet, J.F. Gómez-Aguilar, M.S. Osman, A chaos study of tumor and effector cells in fractional tumor-immune model for cancer treatment, Chaos, Solitons & Fractals 141 (2020) 110321.
[24] D. Baleanu, M. Osman, A. Zubair, N. Raza, O. Abu Arqub, W.X. Ma, Soliton solutions of a nonlinear fractional Sasa-Satsuma equation in monomode optical fibers, Applied Mathematics & Information Sciences 14 (2020) 1-10.
[25] M.A. Akbar, M.A. Kayum, M.S. Osman, A.H. Abdel-Aty, H. Eleuch, Analysis of voltage and current flow of electrical transmission lines through mZK equation, Results in Physics 20 (2021) 103696.
[26] M. Tahir, S. Kumar, H. Rehman, M. Ramzan, A. Hasan, M.S. Osman, Exact traveling wave solutions of Chaffee–Infante equation in (2+ 1)-dimensions and dimensionless Zakharov equation, Mathematical Methods in the Applied Sciences 44 (2021) 1500-1513.
[27] A. Yusuf, S. Qureshi, S.F. Shah, Mathematical analysis for an autonomous financial dynamical system via classical and modern fractional operators, Chaos, Solitons & Fractals 132 (2020) 109552.
[28] S. Qureshi, Monotonically decreasing behavior of measles epidemic well captured by Atangana–Baleanu–Caputo fractional operator under real measles data of Pakistan, Chaos, Solitons & Fractals131 (2020) 109478.
[29] P. Kumar, S. Qureshi, Laplace-Carson integral transform for exact solutions of non-integer order initial value problems with Caputo operator, Journal of Applied Mathematics and Computational Mechanics, 19 (2020) 57-66.
[30] O. Abu Arqub, N. Shawagfeh, Application of reproducing kernel algorithm for solving Dirichlet time-fractional diffusion-Gordon types equations in porous media, Journal of Porous Media 22 (2019) 411-434.
[31] O. Abu Arqub, Fitted reproducing kernel Hilbert space method for the solutions of some certain classes of time-

fractional partial differential equations subject to initial and Neumann boundary conditions, Computers & Mathematics with Applications 73 (2017) 1243-1261.
[32] O. Abu Arqub, Numerical solutions for the Robin time-fractional partial differential equations of heat and fluid flows based on the reproducing kernel algorithm, International Journal of Numerical Methods for Heat & Fluid Flow 28 (2018) 828-856.
[33] O. Abu Arqub, The reproducing kernel algorithm for handling differential algebraic systems of ordinary differential equations, Mathematical Methods in the Applied Sciences 39 (2016) 4549-4562.
[34] O. Abu Arqub, Solutions of time-fractional Tricomi and Keldysh equations of Dirichlet functions types in Hilbert space, Numerical Methods for Partial Differential Equations 34 (2018) 1759-1780.
[35] O. Abu Arqub, Numerical solutions of systems of first-order, two-point BVPs based on the reproducing kernel algorithm, Calcolo 55 (2018) 1-28.
[36] O. Abu Arqub, Z. Odibat, M. Al-Smadi, Numerical solutions of time-fractional partial integrodifferential equations of Robin functions types in Hilbert space with error bounds and error estimates, Nonlinear Dynamics 94 (2018), 1819-1834.
[37] O. Abu Arqub, M. Al-Smadi, An adaptive numerical approach for the solutions of fractional advection-diffusion and dispersion equations in singular case under Riesz's derivative operator, Physica A: Statistical Mechanics and its Applications 540 (2020) 123257.
[38] O. Abu Arqub, M. Al-Smadi, Numerical algorithm for solving time-fractional partial integrodifferential equations subject to initial and Dirichlet boundary conditions, Numerical Methods for Partial Differential Equations 34 (2018) 1577-1597.
[39] O. Abu Arqub, N. Shawagfeh, Solving optimal control problems of Fredholm constraint optimality via the reproducing kernel Hilbert space method with error estimates and convergence analysis. Mathematical Methods in the Applied Sciences 2019 (2019) 1-18.
[40] O. Abu Arqub, M. Al-Smadi, S. Momani, T. Hayat, Application of reproducing kernel algorithm for solving second-order, two-point fuzzy boundary value problems, Soft Computing 21 (2017) 7191-7206.
[41] O. Abu Arqub, Adaptation of reproducing kernel algorithm for solving fuzzy Fredholm-Volterra integrodifferential equations, Neural Computing & Applications 28 (2017) 1591-1610.
[42] O. Abu Arqub, M. Al-Smadi, Atangana–Baleanu fractional approach to the solutions of Bagley–Torvik and Painlevé equations in Hilbert space, Chaos, Solitons & Fractals 117 (2018) 161-167.
[43] O Abu Arqub, B. Maayah, Numerical solutions of integrodifferential equations of Fredholm operator type in the sense of the Atangana–Baleanu fractional operator, Chaos, Solitons & Fractals 117 (2018) 117-124.
[44] O. Abu Arqub, B. Maayah, Fitted fractional reproducing kernel algorithm for the numerical solutions of ABC–Fractional Volterra integro-differential equations, Chaos, Solitons & Fractals 126 (2019) 394-402.
[45] O. Abu Arqub, B. Maayah, Modulation of reproducing kernel Hilbert space method for numerical solutions of Riccati and Bernoulli equations in the Atangana-Baleanu fractional sense, Chaos, Solitons & Fractals 125 (2019) 163-170.
[46] W. Jiang, Z. Chen, A collocation method based on reproducing kernel for a modified anomalous subdiffusion equation, Numerical Methods for Partial Differential Equations 30 (2014) 289-300.
[47] F.Z. Geng, S. P. Qian, S. Li, A numerical method for singularly perturbed turning point problems with an interior layer, Journal of Computational and Applied Mathematics 255 (2014) 97-105.
[48] Y. Lin, M. Cui, L. Yang, Representation of the exact solution for a kind of nonlinear partial differential equations, Applied Mathematics Letters 19 (2006) 808-813.
[49] A. Akgül, A novel method for a fractional derivative with non-local and non-singular kernel, Chaos, Solitons and Fractals 114 (2018) 478-482.
[50] S. Ahmad, A. Ullah, A. Akgül, D. Baleanu, Analysis of the fractional tumour-immune-vitamins model with Mittag–Leffler kernel, Results in Physics 19 (2020) 103559.
[51] I. Siddique, A. Akgül, Analysis of MHD generalized first problem of Stokes' in view of local and non-local fractal fractional differential operators, Chaos, Solitons & Fractals 140 (2020) 110161.
[52] Y. Zhoua, M. Cui, Y. Lin, Numerical algorithm for parabolic problems with non-classical conditions, Journal of

Computational and Applied Mathematics 230 (2009) 770-780.
[53] M. Cui, Y. Lin, Nonlinear numerical analysis in the reproducing kernel space, Nova Science, USA, 2009
[54] A. Berlinet, C.T. Agnan, Reproducing kernel Hilbert space in probability and statistics, Kluwer Academic Publishers, USA, 2004.
[55] A. Daniel, Reproducing kernel spaces and applications, Springer, Basel, Switzerland, 2003.